UNIVERSITY OF CALIFORNIA

Los Angeles

Efficient Generation of Stable Photonic Microwaves by Controlling the Limit-Cycle Oscillations of Optically Injected Semiconductor Lasers

A dissertation submitted in partial satisfaction

of the requirements for the degree

Doctor of Philosophy in Electrical Engineering

by

Mohammad Abdulghani AlMulla

2015

ABSTRACT OF THE DISSERTATION

Efficient Generation of Stable Photonic Microwaves by Controlling the Limit-Cycle Oscillations of Optically Injected Semiconductor Lasers

by

Mohammad Abdulghani AlMulla

Doctor of Philosophy in Electrical Engineering

University of California, Los Angeles, 2015

Professor Jia Ming Liu, Chair

Photonic microwave or millimeter wave (MMW) sources that produce highly stable and broadly tunable microwave frequencies of low phase noise are anticipated for many applications ranging from broadband wireless access networks and satellite communication systems to emerging broadband photonics-based phased-array antennas and radars.

The goal of this dissertation is to investigate and control the characteristics of the generated photonic microwave frequencies induced by an optically injected semiconductor laser. Two ways of controlling the dynamics are considered: through the control of the operational parameters of the optically injected laser system and through the control of the intrinsic parameters of the injected semiconductor laser. Controlling the operating parameters shows limit cycles of period one (P1) and period two (P2) that have reduced sensitivity to intrinsic laser noise and small-signal fluctuations in the operating conditions. The intrinsic parameters of the semiconductor laser, particularly the gain saturation factor, are shown to have

significant effects on the characteristics of the nonlinear dynamics in both the stable-locking and periodic regions. Therefore, this dissertation shows the optimal operating points of the optically injected semiconductor laser for photonic microwave applications.

The dissertation of Mohammad Abdulghani AlMulla is approved.

Chandrashekhar Joshi

Zhilin Qu

Oscar Stafsudd

Jia Ming Liu, Committee Chair

University of California, Los Angeles

2015

This dissertation is dedicated to my family

Table of Contents

List of Figures

ACKNOWLEDGNENTS

First and foremost, all praise be to Allah through whose mercy (and favors) all good things are accomplished.

I would like to express my utmost gratitude to my advisor Professor Jia Ming Liu, for his immense amount of support and guidance during my graduate studies. His words of advice and wonderful stories have kept me motivated through the years and have positively affected me on both a professional and a personal level.

I would also like to extend my gratitude to Dr. Thomas B. Simpson for his help and support. I believe his strong work ethic and insight greatly influenced me, and I am forever grateful.

I wish to thank Professors Chandrashekhar Joshi, Oscar Stafsudd, and Zhilin Qu for their service on my Ph.D. dissertation committee.

I would like to thank members of the Photonic Research Laboratory I-Tan Lin, Chun-Ju Lin, Yu Hsiang Sean Hsu, Yi-Ping Lai and Chun-Ru Fan for their friendship and support. I will always cherish our learning experiences together during my time at UCLA. My gratitude also goes to Mrs. Vida Liu for her encouragement.

I am blessed to have a wonderful, loving, and supportive family. I thank my parents, my mother especially, my first teacher, for her constant prayers and support throughout my time in the United States. I thank my brother, Tariq, and sisters, Dalal, Hissa, and Hala for their support and encouragement.

Finally, I would like to acknowledge the financial support from Kuwait University throughout my graduate studies. Without them, the work done here would not be possible.

VITA

2003-2008	B.S., Department of Electrical Engineering, Kuwait University, Kuwait
2009-2012	M.S., Department of Electrical Engineering, University of California, Los Angeles
2012-2015	Graduate Student Researcher, Department of Electrical Engineering, University of California, Los Angeles, USA

PUBLICATIONS

M. AlMulla, J. M. Liu, "Stable Periodic Dynamics of Reduced Sensitivity to Perturbations in Optically Injected Semiconductor Lasers," *IEEE Journal of Selected Topics in Quantum Electronics*, vol. 21, pp. 1-8, 2015.

M. AlMulla and J. M. Liu, "Frequency-stabilized limit-cycle dynamics of an optically injected semiconductor laser," *Applied Physics Letters*, vol. 105, p. 011122 2014.

T. B. Simpson, J. M. Liu, **M. AlMulla**, N. G. Usechak, and V. Kovanis, "Tunable Oscillations in Optically Injected Semiconductor Lasers With Reduced Sensitivity to Perturbations," *Journal of Lightwave Technology*, vol. 32, pp. 3749-3758, 2014.

C. J. Lin, **M. AlMulla**, and J. M. Liu, "Harmonic Analysis of Limit-Cycle Oscillations of an Optically Injected Semiconductor Laser," *IEEE Journal of Quantum Electronics,* vol. 50, pp. 815-822, 2014.

M. AlMulla and J. M. Liu, "Effects of the Gain Saturation Factor on the Nonlinear Dynamics of Optically Injected Semiconductor Lasers," *IEEE Journal of Quantum Electronics,* vol. 50, pp. 158-165, 2014.

T. B. Simpson, J. M. Liu, **M. AlMulla**, N. G. Usechak, and V. Kovanis, "Limit-Cycle Dynamics with Reduced Sensitivity to Perturbations," *Physical Review Letters,* vol. 112, p. 23901, 2014.

M. AlMulla, X. Q. Qi, and J. M. Liu, "Dynamics Maps and Scenario Transitions for a Semiconductor Laser Subject to Dual-Beam Optical Injection," *IEEE Journal of Selected Topics in Quantum Electronics,* vol. 19, p. 1501108, 2013.

T. B. Simpson, J. M. Liu, **M. AlMulla**, N. Usechak, and V. Kovanis, "Linewidth Sharpening via Polarization-Rotated Feedback in Optically-Injected Semiconductor Laser Oscillators," *IEEE Journal of Selected Topics in Quantum Electronics,* vol. 19, p. 1500807, 2013.

T. B. Simpson, J. M. Liu, **M. AlMulla**, N. Usechak, and V. Kovanis, "Tunable photonic microwave oscillator self-locked by polarization-rotated optical feedback," in *Frequency Control Symposium (FCS), 2012 IEEE International*, 2012, pp. 1-5.

CHAPTER 1

Introduction

1.1 Motivation

Microwave Photonics is an inter-disciplinary field of study that concerns interactions between microwave and optical waves for the generation, processing, control and, distribution of microwave, millimeter-wave, and THz-frequency signals. The main advantage of microwave photonic systems relative to conventional electrical transmission systems include: compact size, reduced cost and weight, low attenuation across the microwave modulation frequency range, immunity to electromagnetic interference, low dispersion, and high data throughput [1, 2, 3]. The field of microwave photonics also has the advantage of using photonic technologies to provide functions in microwave systems that are otherwise unavailable [4]. Many methods have been developed to generate stable photonic microwaves, each with certain advantages and limitations [3, 5]. An ideal photonic microwave system generates high-microwave-frequency signals of low phase noise over a wide frequency-tuning range. Furthermore, generating these photonic microwave signals with relatively simple or no required electronics with a single sideband modulation scheme is also desirable.

Direct modulation of a laser is the simplest photonic microwave frequency generation technique where only a microwave signal and the laser are required [6]. They are limited by the laser relaxation resonance frequency [7]. Currently direct modulation of a semiconductor laser can reach a frequency up to 30 GHz for optical-transmission wavelengths [8]. To overcome the limitation set by the relaxation resonance frequency of the laser, external modulation by a Mach–Zehnder modulator (MZM) or an electro-absorption modulator (EAM) is

used on the semiconductor laser output. A high microwave frequency of 40 GHz with low phase noise without special design requirements on the system was achieved [9, 10]. Besides the added complexity on the system, the major drawback of external modulation is its high insertion loss, which requires a strong pump laser as an input [11]. To simplify the electronics, optical heterodyne where the beat signal of two optical beams at different frequencies is used to generate high frequency photonic microwaves in the terahertz range with the only limit being the photodetector frequency response. The beat signal of high microwave/terahertz frequencies come with poor stability due to the two optical beams being not phase correlated [12]. To reduce the phase noise one can lock the phase of the two lasers by an optical phase-locked loop [13, 14]. Optical injection can also be used to augment on the aforementioned methods, creating a higher modulation bandwidth in direct modulation [15] or added to the optical heterodyne technique by locking the two slave lasers to different modulation sidebands of a third modulated master laser [16]. Other techniques with phase correlation are established such as mode-locked lasers [17, 18], optoelectronic oscillators [19], or dual-mode semiconductor lasers [20, 21]. Although such techniques offer reduced phase noise, they are not frequency tunable.

Recent developments in the field of nonlinear dynamics of semiconductor lasers have shown significant advances in the understanding of the dynamic states, which in turn makes it possible to control the dynamics. Limit-cycle dynamics [22] induced by perturbing a semiconductor laser is one avenue where photonic microwaves with favorable characteristics is demonstrated through the control of the nonlinear dynamics [23, 24].

1.2 Background

Nonlinear dynamics of lasers have been a topic of intense research since their discovery in lasers by Haken [25] in analogy to the nonlinear dynamics in convective fluids found by Lorenz [26]. Semiconductor lasers are considered class B lasers, where the population decays slowly, so that the dynamics is described by two coupled rate equations which are still insufficient to yield dynamic instabilities [27]. They can invoke nonlinear dynamics only through increasing the number of degrees of freedom by at least one [28]. The ability to invoke such dynamics in a semiconductor laser stems from that the gain is a function of the optical field and carrier density [7, 29, 30]. Therefore, introducing a perturbation source to the semiconductor laser can induce instabilities [31, 32]. Various perturbation methods were used to invoke nonlinear dynamics in a semiconductor laser such as but not limited to: strong current modulation [32, 33, 34, 35, 36, 37], optical injection [38, 39, 40, 41, 42, 43, 44, 45], dual-beam optical injection [46, 47, 48, 49, 50, 51, 52], optoelectronic feedback [53, 54, 55, 56, 57, 58], optical feedback [59, 60, 61, 62, 63], hybrid systems [64, 65, 66, 67], semiconductor lasers with saturable absorbers [68, 69, 70], and coupled lasers [71, 72, 73, 74, 75, 76].

Numerous nonlinear dynamics invoked by the aforementioned perturbation techniques are useful for many applications ranging from cryptography to microwave photonics and instrumentation. These dynamics include stable locking [77], periodic oscillation [45, 78, 79], quasi-periodicity [58], chaotic oscillation [80, 81], and chaotic pulsation [82].

The focus of this dissertation is on limit-cycle or period-one oscillations induced by optically injected semiconductor lasers. Limit-cycle dynamics addressed here are self-sustained oscillations that are generated due to undamping the relaxation resonance of the semiconductor laser through continuous-wave optical injection [22]. Optically injected sem-

iconductor lasers operated in the periodic region offer photonic microwaves that are generated by an all-optical method, are frequency tunable, have single-sideband modulation, and have no optical loss, making them an attractive microwave generation method for many applications.

The main drawback of the generated photonic microwave is its relatively large linewidth, which arises from the intrinsic laser noise and from small-signal fluctuations in the bias currents and the temperatures of the two lasers [83, 84, 85]. Many efforts have been carried out to reduce this linewidth by stabilizing the P1 frequency. A double-locking technique was implemented to stabilize the P1 frequency by using an externally applied microwave that is tuned to the P1 oscillation frequency or its subharmonics [86, 87, 88, 89]. Adding a phase-locked loop to the optical injection system to lock the phase of the microwave subcarrier to an external microwave further stabilized the P1 oscillation [90]. A self-locking method using optoelectronic feedback to lock the P1 frequency generated by optical injection to a delayed replica of the P1 frequency narrowed the P1 oscillation frequency as well [91]. Recently the all-optical version of the self-locking method was demonstrated using a polarization-rotated optical feedback or a dual-loop optical feedback [92, 93, 94, 95]. Dual-beam optical injection operated in Scenario AB [50], where the injection parameters of one of the injection fields are tuned to the stable injection locking region [49], generates stable P1 microwave frequencies without complex electronics [96, 97].

The goal of this dissertation is to stabilize the photonic microwave frequencies generated by an optically injected semiconductor laser through the control of the system operational parameters and the intrinsic laser parameters.

1.3 Dissertation Outline

After this introductory chapter a description of the experimental setup and the theoretical model used in this work are described in Chapter 2. In Chapter 3, limit-cycle oscillations with low-sensitivity to fluctuations in one or more operational parameters are discussed for limit cycles of period-one (P1) and period-two (P2) dynamics. Two-dimensional mappings of the nonlinear dynamics of an optically injected semiconductor laser and points of reduced sensitivity to perturbation are also demonstrated, along with a discussion on their relationship. In Chapter 4, studies on the effects of the gain saturation factor on the characteristics of the photonic microwaves generated by the optically injected semiconductor laser are discussed. Finally, a summary of our results and future research in this field are presented in Chapter 5.

CHAPTER 2

Optical Injection System: Theory and Experiment

The optical injection system exhibits rich and complex nonlinear dynamics with its relatively simple experimentally setup. These nonlinear dynamics can be qualitatively and quantitatively recovered through a well-established theoretical model relating the circulating optical field and the free carriers of the gain medium. Therefore, the optical injection system is used not only for application purposes but also as a way to understand nonlinear dynamics in general where both theory and experiment are accessible with excellent agreement. In this chapter, the experimental setup and the numerical calculation used throughout this dissertation are described.

2.1 Introduction

Photonics microwave are anticipated for many applications. These applications include lidar detection, phased-array radars, ultrafast noninvasive measurements, and imaging. Another major application is radio-over-fiber (RoF) communication which has become a commercial reality, and the need for higher bandwidth capacity and ability for signal processing without microwave electronic complexity is still in the research phase. The period-one (P1) dynamics of a semiconductor laser induced by optical injection provide an all-optical microwave generation technique that avoids the limitation set by microwave electronics and electrical parasitics. The P1 frequencies are broadly tunable by simply changing the temperatures or bias currents of the two lasers. They offer microwave frequencies up to ten times the relaxation resonance frequency of the solitary laser, reaching frequencies of 100 GHz. The P1 dy-

namics induced by semiconductor lasers also have a natural single-sideband optical spectrum, making them immune to chromatic dispersion-induced microwave power penalty. Recent studies also showed all-optical signal processing methods utilizing the characteristics of the P1 and P2 dynamics. A frequency-modulated master laser can optically inject a slave laser into a P1 dynamic for double-sideband to single-sideband conversion and power amplification [98, 99]. The emergence of new optical frequency components in the P1 and P2 dynamics was utilized for frequency conversion [100, 101]. All-optical techniques for modulation format conversion were investigated to reduce the complexity of the overall system by bypassing the electronics [102, 103]. A tunable passband photonic microwave filter using a similar setup has also been realized [104]. These advantages of the P1 and P2 dynamics induced by optically injected semiconductor lasers make them a suitable photonic microwave generation technique.

2.2 Experimental Setup

A schematic of the experimental setup is shown in Fig. 2.1. Three single-mode, distributed feedback lasers (DFB) operating at 1.3μm wavelengths are used in this experiment (Bookham Technology LC131). Each laser is current and temperature stabilized by a modular controller (Newport 8000/8008). The slave laser has a current threshold of 18 mA and is operated at constant current and temperature of 40 mA and 18 ºC, respectively. The master laser has a current threshold of 15 mA and is operated around a current of 116 mA at a temperature of 15.5 ºC. The master laser

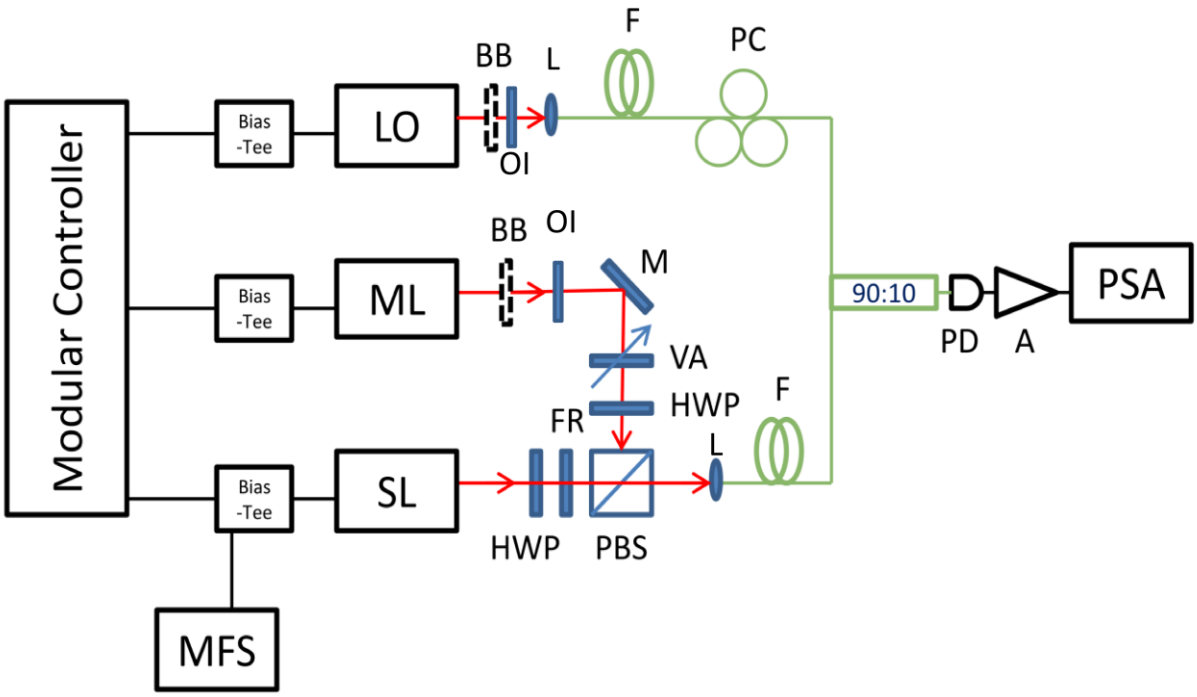

Figure 2.1: Schematic of the optical injection system. SL: slave laser; ML: master laser; LO: local oscillator laser; MFS: microwave frequency synthesizer F: optical fiber; OI: optical isolator; M: Mirror; PBS: polarizing beam splitter; VA: variable attenuator; HWP: half wave plate; FR: Faraday rotator; BB: beam blocker; L: lens; PC: polarization controller; PD: photodetector; A: amplifier and PSA: power spectrum analyzer.

temperature is adjusted around 15.5 ºC for broad frequency changes and then the current is adjusted around 116 mA for fine frequency tuning. The local oscillator (LO) laser has a threshold of 15 mA and is operated around a current of 44 mA at a temperature of 16 ºC. The LO laser is used for heterodyne detection, and its frequency is tuned by varying its temperature and current depending on the operating conditions. A free-space circular configuration is used to inject the light from the master laser oscillating at a frequency ν_{ML} into the slave laser oscillating at a frequency ν_{SL}. The frequency difference between the two laser, $f = \nu_{ML} - \nu_{SL}$, is the detuning frequency. Throughout this dissertation, an optical frequency is referred to as ν, while a microwave frequency is referred to as f. The circular configuration consists of a mirror (M), a variable attenuator (VA), two half-wave plates (HWP), a polarizing beam splitter (PBS), and a Faraday rotator (FR). The injection strength parameter, ξ, is proportional to the ratio of the electric field of the injection signal and that of the free-running slave laser. The square of the injection parameter is proportional to the injection power actually received by the slave laser. A power meter is used just before the slave laser to measure the relative power injected into the slave laser. To tune the injection strength, either the VA is adjusted or the master laser polarization is changed before the PBS through the first HWP. The Faraday rotator and the second HWP are used to adjust the polarization state of the slave laser such that the maximum amount of power transmits through the PBS into the coupling lens. The polarization state of the injection signal has to be the same as that of the slave laser output right before the slave laser. Note that the Faraday rotator rotates the linear polarization of an optical field by 45 degrees along the same sense no matter which side of the rotator the optical field is incident from [7]. The output is then coupled into a single-mode fiber and sent to a 35-GHz photodiode (PD) (Discovery Semiconductors DSC20S-

3-FC) to convert the optical signal into an electrical signal. The power spectrum is then recorded by a microwave spectrum analyzer that has a bandwidth of 26.5 GHz (HP E4407B) after being amplified by a RF amplifier (HP 83006A) that has a gain of 20 dB and a bandwidth of 26.5 GHz. A microwave frequency synthesizer (MFS) (HP 83620A) can be used to apply weak current modulation to either the slave laser or master laser bias currents.

To get a high-resolution optical spectrum, an optical heterodyne scheme is used. Removing the Beam Blocker (BB) in front of the LO laser allows the detection of the optical spectrum. The LO laser frequency is fixed at a frequency close to or in between the spectral peaks of the generated dynamic. The LO laser is mixed with the generated signal from the optically injected laser through a 90:10 fiber coupler. The generated output on the PSA is a combined power spectrum of the optically injected slave laser and the heterodyne spectrum of the mixing of the injected slave laser output and the LO laser. Since the LO laser output is essentially monochromatic and can be polarization controlled, its power spectrum has no spectral features that contribute to our optical spectrum or degrade our results. Given that the spectral features do not overlap, the resolution of this technique is limited by the linewidth of the LO oscillator laser only. The second BB in front of the master laser is used to identify the frequency spectral components of the mixing of the slave laser frequency and LO laser. To identify the master laser frequency component in the heterodyne spectra, the residual power of the master laser output after the PBS is mixed with the LO laser while the slave laser frequency is blocked or turned off.

2.3 Theoretical Model

A single-mode semiconductor laser is a class B laser since the relaxation time of the material polarization is much shorter than the carrier and photon lifetimes. Consequently, it can be adequately described by two equations, one for the complex laser field and the other for the carrier density. The laser under optical injection with modulation on the slave laser bias current or the master laser output can be described by a well-established set of coupled nonlinear rate equations [105]:

$$\begin{aligned}\frac{\mathrm{d}A}{\mathrm{d}t} = &\left[-\frac{\gamma_\mathrm{c}}{2}+\mathrm{i}(\omega_0-\omega_\mathrm{c})\right]A+\frac{\Gamma}{2}g(N,|A|)A \\ &+\eta\left[1+m_\xi\cos(2\pi f_\xi t)\right]A_\mathrm{i}\exp(-\mathrm{i}(\Omega_\mathrm{i}t+m_f\cos(2\pi f_f t)))\end{aligned} \tag{2.1}$$

$$\frac{\mathrm{d}N}{\mathrm{d}t} = \frac{J+J_\mathrm{m}\cos(\Omega_\mathrm{m}t)}{ed}-\gamma_\mathrm{s}N-\frac{2\varepsilon_0 n^2}{\hbar\omega_0}\mathrm{Re}\left[g(N,|A|)\right]|A|^2 \tag{2.2}$$

where A is the complex intracavity field amplitude at the free-running slave laser angular frequency ω_0, γ_c is the cold cavity decay rate, ω_c is the cold cavity angular frequency, Γ is the confinement factor that relates the overlap of the oscillating mode with the gain medium, η is the injection coupling rate, A_i is the injection field amplitude, $\Omega_\mathrm{i} = 2\pi f_\mathrm{i}$ is the detuning frequency of the master laser with respect to ω_0. In the equation describing the population density of the gain medium, N is the charge carrier density, J is the injection current density, e is the electronic charge, d is the active layer thickness, γ_s is the spontaneous carrier relaxation rate, ε_0 is the free-space permittivity, n is the refractive index, and $\hbar$ is the reduced Planck's constant. The complex gain, $g(N, |A|)$, varies about the free-running, steady-state operating point as a function of the carrier density and the intracavity photon density, S [7]:

$$g(N,|A|) = (1-\mathrm{i}b)\mathrm{Re}\left[g(N_0,A_0)\right] + (1-\mathrm{i}b)\gamma_\mathrm{n}\frac{N-N_0}{S_0} - (1-\mathrm{i}b')\gamma_\mathrm{p}\frac{S-S_0}{\Gamma S_0} \qquad (2.3)$$

where γ_n is the differential carrier relaxation rate, γ_p is the nonlinear carrier relaxation rate, and N_0 and S_0 are respectively the steady-state values of N and S when the slave laser is free running. The intracavity photon density, S, is related to the laser field amplitude by [42]:

$$S = \frac{2\varepsilon_0 n^2}{\hbar\omega_0}|A|^2 . \qquad (2.4)$$

Notice the gain in equation (2.3) depends on both the carrier density and the intracavity photon density. The nonlinear gain or gain saturation which is represented by the last term in equation (2.3) is generally attributed to spectral hole burning and carrier heating and is often neglected, although experiments show gain saturation to be of crucial importance in describing the dynamics of the semiconductor laser [106]. Equations (2.1) and (2.2) can be normalized by taking $a_\mathrm{r}+\mathrm{i}a_\mathrm{i} = A/|A_0|$ and $1+\tilde{n} = N/N_0$, where A_0 is the free-running A, to yield three real equations:

$$\begin{aligned}\frac{da_\mathrm{r}}{dt} = \frac{1}{2}\left[\frac{\gamma_\mathrm{c}\gamma_\mathrm{n}}{\gamma_\mathrm{s}\tilde{J}}\tilde{n}\left(a_\mathrm{r}+ba_\mathrm{i}\right) - \gamma_\mathrm{p}\left(a_\mathrm{r}^2+a_\mathrm{i}^2-1\right)\left(a_\mathrm{r}+b'a_\mathrm{i}\right)\right] \\ + \xi\left[1+m_\xi\cos(2\pi f_\xi t)\right]\gamma_\mathrm{c}\cos(2\pi ft + m_f\cos(2\pi f_f t))\end{aligned} \qquad (2.5)$$

$$\begin{aligned}\frac{da_\mathrm{i}}{dt} = \frac{1}{2}\left[\frac{\gamma_\mathrm{c}\gamma_\mathrm{n}}{\gamma_\mathrm{s}\tilde{J}}\tilde{n}\left(-ba_\mathrm{r}+a_\mathrm{i}\right) - \gamma_\mathrm{p}\left(a_\mathrm{r}^2+a_\mathrm{i}^2-1\right)\left(-b'a_\mathrm{r}+a_\mathrm{i}\right)\right] \\ - \xi\left[1+m_\xi\cos(2\pi f_\xi t)\right]\gamma_\mathrm{c}\sin(2\pi ft + m_f\cos(2\pi f_f t))\end{aligned} \qquad (2.6)$$

$$\frac{d\tilde{n}}{dt} = -\left[\gamma_s + \gamma_n\left(a_r^2 + a_i^2\right)\right]\tilde{n} - \gamma_s\tilde{J}\left(a_r^2 + a_i^2 - 1\right) + \frac{\gamma_s\gamma_p}{\gamma_c}\tilde{J}\left(a_r^2 + a_i^2\right)\left(a_r^2 + a_i^2 - 1\right) + \gamma_s m_{\tilde{J}}(1+\tilde{J})\cos(2\pi f_{\tilde{J}} t) \tag{2.7}$$

where $\tilde{J} = (J / ed - \gamma_s N_0) / \gamma_s N_0$ is the normalized bias above the threshold current and $\xi = \eta|A_i| / \gamma_c|A_0|$ is the dimensionless injection strength. For some of our results, modulation is applied to either the slave laser bias current or the master laser output. The modulation indices, $m_{\tilde{J}}$, m_ξ, and m_f, and the modulation frequencies, $f_{\tilde{J}}$, f_ξ, and f_f, represent the modulation added to the system with the subscripts $\tilde{J}$, ξ, and f, respectively, indicating current modulation on the slave laser, injection-strength modulation on the master laser output, and detuning-frequency modulation on the master laser output.

The dynamical parameters used in this paper have been experimentally extracted using a well-established four-wave mixing technique [107]. Their values used in this study are experimentally measured parameters of a InGaAsP/InP DFB semiconductor laser at 1.3 μm wavelength [15]: $b = 3.2$, $\gamma_c = 5.36 \times 10^{11}$ s^{-1}, $\gamma_s = 5.96 \times 10^9$ s^{-1}, $\gamma_n = 7.53 \times 10^9$ s^{-1}, and $\gamma_p = 1.91 \times 10^{10}$ s^{-1} for a normalized bias current of $\tilde{J} = 1.222$. These parameters give a relaxation resonance frequency of 10.25 GHz. All intrinsic parameters are kept constant at their experimentally measured values throughout this dissertation except for b', which is varied in Chapter 4 from its experimentally measured value of $b = b' = 3.2$ for this laser to study its effects on various dynamical characteristics of a semiconductor laser. Equations (2.5)-(2.7) are numerically solved using second-order Runge-Kutta integration for a duration longer than 1 μs for each time series with an integration time step of 2.4 ps. The optical and power spectra of the slave laser output are found by taking the Fourier transform of the time series

$a(t)$ and $|a(t)|^2$, respectively. The laser noise has been omitted from the model so that the spectral peaks can be easily identified for clear comparison of various spectra.

CHAPTER 3

Controlling the Operational Parameters for Stable Photonic Microwave Generation

This chapter investigates the limit cycles of P1 and P2 dynamics induced by an optically injected semiconductor laser. Through the control of the operation parameters, namely, the injection strength, detuning frequency, and bias current the limit cycle frequency can have reduced sensitivity to perturbations and intrinsic laser noise. Two-dimensional mapping of the limit-cycle frequency are demonstrated showing low-sensitivity regions for efficient microwave frequency generation.

3.1 Introduction

The main purpose of any oscillator is to generate a stable oscillation frequency. Conventionally, to achieve such target the oscillator is operated in its linear, harmonic region with the highest possible signal-to-noise ratio to reduce its phase noise. To surpass this paradigm recent development showed that the deleterious effects in the nonlinear region of oscillators could be used to stabilize the generated signal. Cancellation of nonlinear effects to stabilize a system by reducing phase noise has been demonstrated in micromechanical and nanoelectromechanical nonlinear oscillators [108, 109, 110]. These nonlinear oscillators, characterized by the Duffing equation, undergo such cancellation effects at critical points where the slope of the amplitude-frequency or phase-frequency curve is infinite [111].

Limit cycles generated by nonlinear oscillators can be described by a closed orbit in the phase space of its dynamical variables [22]. The linewidth of such self-sustained oscillation is zero and only becomes nonzero in the presence of noise. The nonzero linewidth of a perturbed nonlinear oscillator comes from its autonomous nature, where the oscillator responds to perturbation by spiraling back into the limit cycle but at a different phase. For the limit-cycle dynamics induced by optical injection of a semiconductor laser, fluctuations in the control parameters and the intrinsic laser noise perturb the system and broaden the linewidth. The intrinsic optical noise and carrier noise of a laser can be modeled as stochastic source terms in the optical-field and carrier-density equations of the laser [112, 113]. Through a proper choice of the operating condition in the optical injection system, fluctuations in the limit-cycle frequency due to fluctuations in the control parameters, spontaneous emission noise, and carrier noise can be mitigated by taking advantage of the oscillator nonlinearities. Distinct types of these inherently low-sensitivity (LS) points are revealed showing reduced sensitivity to different perturbations.

To identify these LS points, a weak modulation signal is added to the optical injection system, operated in a P1 or P2 dynamic, to either the bias current of the slave laser or the output of the master laser. The power spectrum, shown in Fig. 3.1, demonstrates the representative modulated P1-frequency carrier, where two modulation sidebands appear around the P1 oscillation frequency, f_0, and around each of its harmonics (not shown). The magnitudes of the modulation sidebands with respect to the P1-frequency carrier, measured in dBc, are a manifestation of the P1 frequency stability at different operating conditions. Therefore, a modulation is added to the

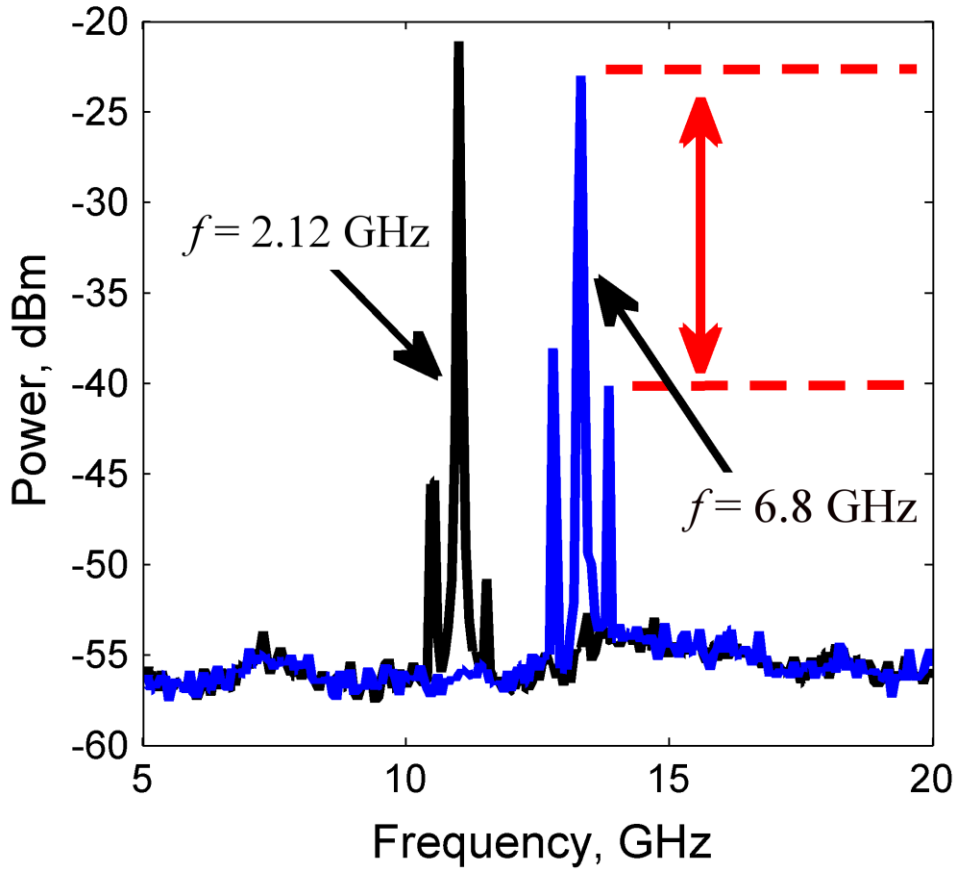

Figure 3.1: Power spectrum of the amplified photodiode signal monitoring the output of the current modulated optically-injected laser operating in the P1 regime where its output power oscillates at the fundamental resonance frequency for a fixed ξ and f = 2.12 GHz (black) and f = 6.8 GHz (blue). The spectrum displays a strong frequency component at the frequency, f_0, and two modulation sidebands around f_0. The magnitudes of the modulation sidebands with respect to the P1-frequency carrier, measured in dBc, are a measure of the P1 frequency stability.

optical injection system as a test of the P1 frequency stability through the measure of the modulation sideband suppression with respect to the P1-frequency carrier. The low-sensitivity points with respect to the fluctuations in the injection strength (LS_{ξ}), the detuning frequency (LS_{f}), and the slave-laser bias current ($LS_{\hat{\jmath}}$) are identified by modulating the corresponding control parameters.

3.2 Period-One Low-Sensitivity Points

3.2.1 Low Sensitivity to Injection-Strength Fluctuations

Limit cycles of P1 oscillations with low-sensitivity to fluctuations in the injection strength, LS_{ξ}, show reduced sensitivity to the effects of fluctuations in the temperatures or bias currents of the two lasers on the injection strength (i.e. effects of laser-intensity fluctuations). The LS_{ξ} points also exhibit reduced disturbances from spontaneous emission noise on the laser field amplitude. Consequently, the frequency of the limit cycles at these sensitivity points is still sensitive to the effects of laser-frequency fluctuations, slave laser bias-current fluctuations, and carrier noise. These points are located at a local P1 frequency extrema with respect to the injection strength.

To identify the LS_{ξ} points, a weak amplitude modulation is added to the master laser field amplitude to mimic fluctuations in the injection strength. The amplitudes of the modulation sidebands with respect to the P1-frequency amplitude quantify the P1 frequency stability in dBc. Spontaneous emission noise and carrier noise induced fluctuations can also be considered as amplitude and phase modulations of the coherent signal and therefore are tested in a similar manner [112].

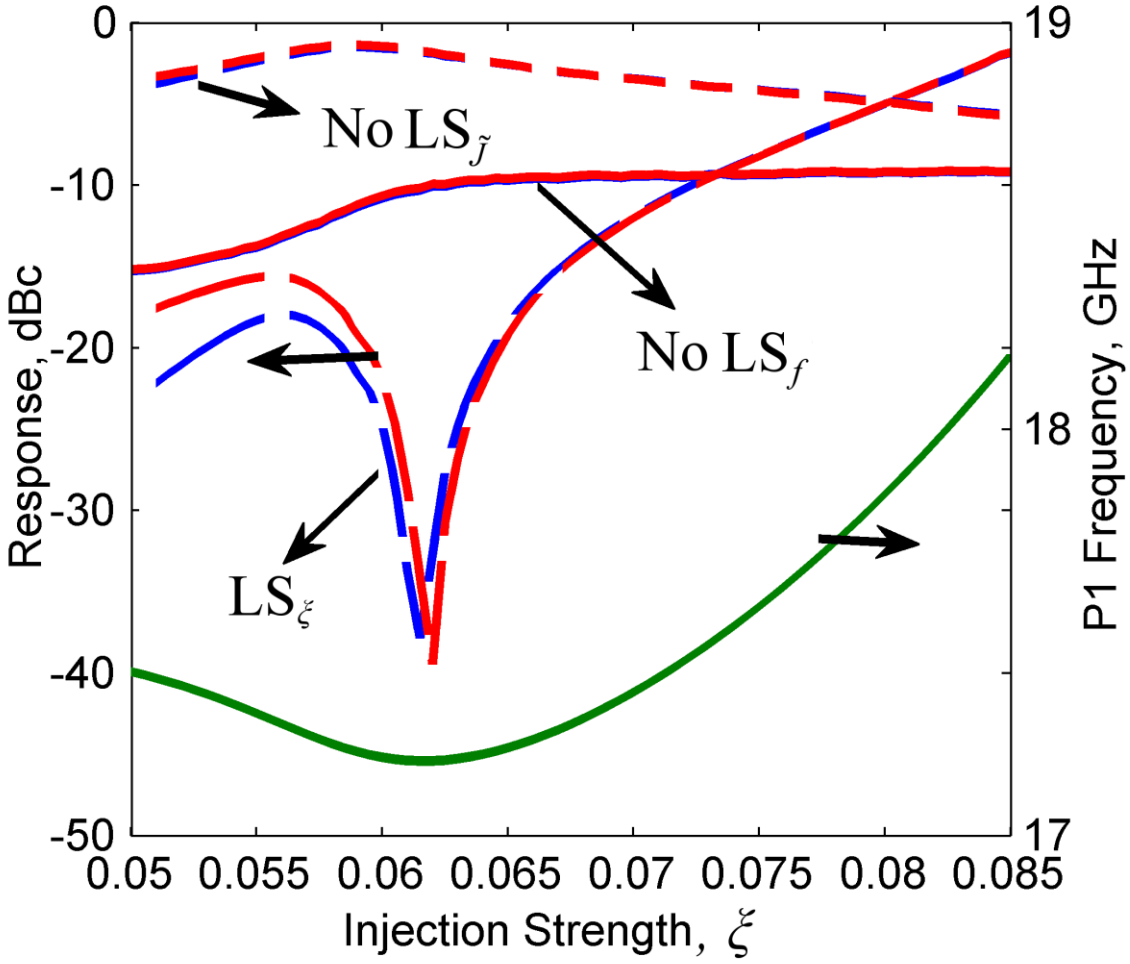

Figure 3.2: Responses of the positive (blue) and negative (red) modulation sidebands of the P1-frequency carrier near a local minimum of the P1 frequency (green) with respect to the injection strength at fixed f = 10 GHz and $\tilde{J}$ = 2.9. To identify an LS$_f$ point, a weak detuning-frequency modulation at f_f = 100 MHz is applied (solid curves). To identify an LS$_\xi$ point, a weak injection-strength modulation at f_ξ = 100MHz is applied (long dashed curves). To identify an LS$_{\tilde{J}}$ point, a weak bias-current modulation at $f_{\tilde{J}}$ = 100MHz is applied (short dashed curves).

Figure 3.2 shows the responses of the modulation sidebands around a local minimum of the P1 frequency with respect to ξ. The injection strength is swept from ξ = 0.05 to ξ = 0.085, while the other operating parameters are held constant at f = 10 GHz and $\tilde{J}$ = 2.9, creating a P1 frequency with a local minimum at ξ = 0.062 as a function of ξ. Two sharp dips in the responses of the modulation sidebands with respect to the P1-frequency carrier are observed at the local P1 frequency minimum, when a weak amplitude modulation to the master laser output is applied at f_ξ = 100 MHz, indicating an LS_ξ point (long dashed curves). The responses of the modulations sidebands show no dips when a weak frequency modulation to the master laser is applied at f_f = 100 MHz (solid curves) or when bias current modulation to the slave laser bias current is applied at f_J = 100 MHz (short dashed curves). This indicates that at an LS_ξ the detuning-frequency and bias-current fluctuations still effect the P1 frequency stability. The modulation sidebands are normalized to the P1-frequency carrier because the power of the P1-frequency spectral line varies as the operational parameters change [23]. A P1 frequency extremum with respect to ξ can be found at different combinations of the operational conditions ξ, f, and $\tilde{J}$. Therefore, two-dimensional maps with respect to ξ -f and $\tilde{J}$ - f are calculated to show the LS_ξ regions.

Figures 3.3(a) and (b) show the LS_ξ regions characterized by suppressed responses of the positive and negative modulation sidebands, respectively, when the bias current is fixed at $\tilde{J}$ = 1.222 while ξ and f are varied. The Hopf bifurcation curve (thick black curve) separates the stable locking region (uncolored) from the periodic dynamics region (colored). The contour curves represent the P1 frequency in GHz, whereas the colored regions show the amount of suppression of the modulation sidebands relative to the P1-frequency amplitude in dBc. Chaos regions are highlighted in black.

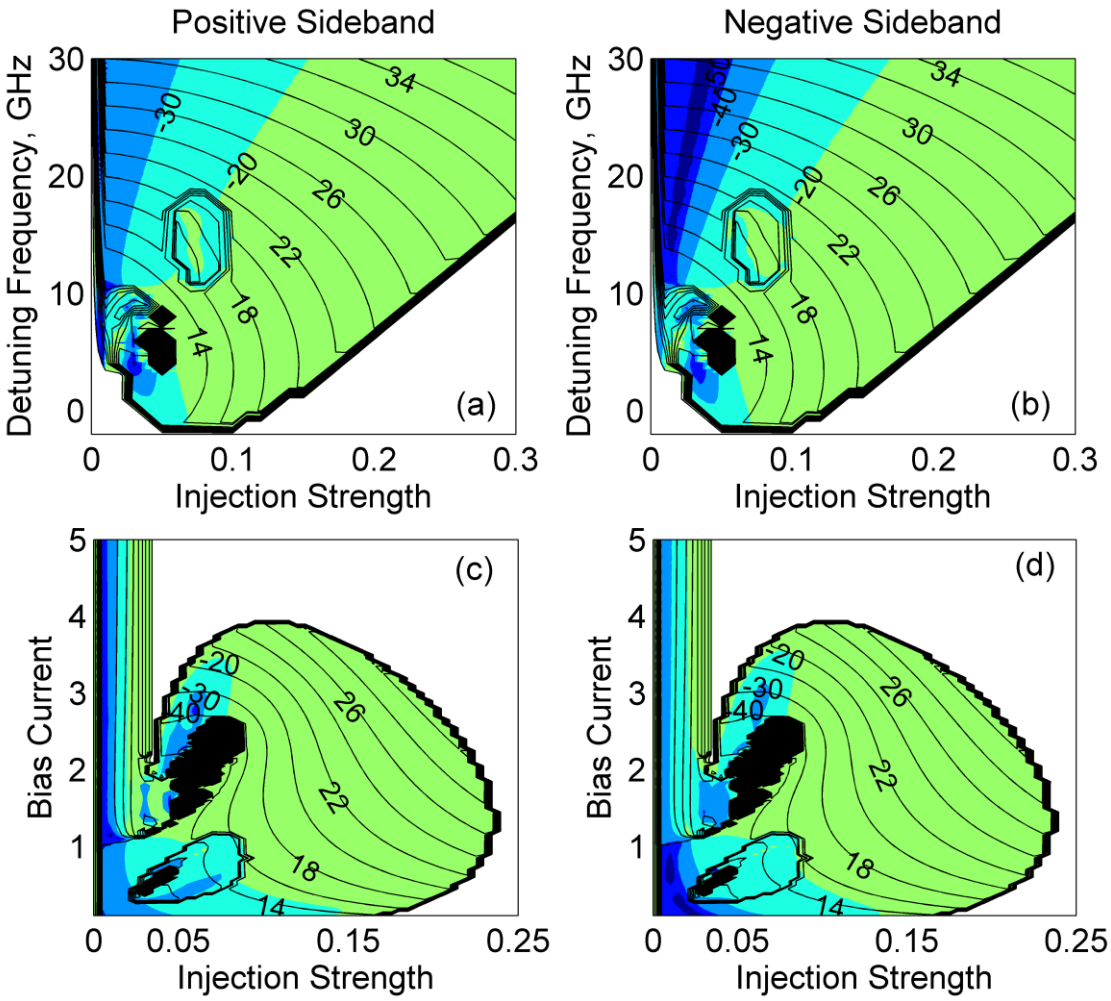

Figure 3.3: Mapping of the LS_{ξ} regions obtained by applying a weak modulation on the injection strength at f_{ξ} = 500 MHz. The maps are plotted as a function of the injection strength and detuning frequency in (a) and (b), and as a function of the injection strength and bias current in (c) and (d). The contour curves represent the P1 and P2 frequency, in GHz. The colored regions represent the amount of sideband suppression with respect to the P1-frequency amplitude, in dBc, under a weak modulation on the injection strength for the positive (left column) and negative (right column) sidebands. Stable locking (uncolored region) and chaotic dynamics (black regions) are shown across the Hopf bifurcation curve (thick black curve). P1 dynamics and P2 dynamics are separated by the period-doubling bifurcation (dense curve).

The period-doubling bifurcation (dense curve) separates the P1 region from the P2 region. An LS_ξ region (dark blue) is found bounded by the Hopf bifurcation curve and the period-doubling curve close to the chaotic dynamics. The existence of these LS_ξ points is due to local P1 frequency minima with respect to ξ that arise just before the period-doubling bifurcation. Other LS_ξ points are found at small injection strengths and high detuning frequencies, where the P1 dynamics have relatively low power [29]. The responses of the negative modulation sideband at small injection strengths and large detuning frequencies, shown in Fig 3.3(b), appear to be more suppressed than their positive counterparts in Fig 3.3(a). This difference is attributed to the shift of the dips in the responses of the modulation sidebands away from the P1 frequency extremum as the modulation frequency is increased. At higher modulation frequencies, the negative and positive sidebands shift away from the P1 frequency extremum in opposite directions (see supplementary material in [83]). Reducing the modulation frequency to 100 MHz in Fig. 3.3(b) shifts the dip in the response of the negative modulation sideband closer to the P1 frequency extremum.

Figures 3.3(c) and (d) show the LS_ξ regions characterized by suppressed responses of the positive and negative modulation sidebands, respectively, when the detuning frequency is fixed at f = 10 GHz while ξ and $\tilde{J}$ are varied. The Hopf bifurcation curve (thick black curve) separates the stable locking region (uncolored) from the periodic dynamics region (colored). The contour curves represent the P1 frequency in GHz, whereas the colored regions show the amount of suppression of the modulation sidebands relative to the P1-frequency amplitude in dBc. Chaos regions are highlighted in black. The period-doubling bifurcation (dense curve) separates the P1 region from the P2 region. When $\tilde{J}$ is varied, changes in the relaxation rates γ_n and γ_p have to be taken into consideration in the theoretical model because γ_n

and γ_p vary linearly with $\tilde{J}$, whereas the other intrinsic parameters are independent of $\tilde{J}$ [107]. Varying the bias current with suppressed nonlinear gain in the theoretical model creates discrepancies between the theoretical and experimental results [114]. The reason for such discrepancies is because of the competition between the differential gain effect and the nonlinear gain effect, both of which vary linearly with $\tilde{J}$ [115]. The region where the P1 frequency undergoes a local P1 frequency minimum with respect to ξ in Figs. 3.3(c) and (d) is where LS_ξ are identified. The P1-frequency minima, bounded by the Hopf bifurcation curve and the chaos region, are due to the competition between Adler-type pulling and red shifting of the cavity resonance [83, 85].

No LS_ξ points are found in the dynamics maps when the injection strength is fixed at ξ = 0.15 while f and $\tilde{J}$ are varied because no minima of the P1 frequency with respect to ξ occur.

3.2.2 Low Sensitivity to Detuning-Frequency Fluctuations

P1 oscillations with reduced sensitivity to fluctuations in the detuning frequency, LS_f, show reduced sensitivity to the effects of fluctuations in the temperatures and bias currents of the two lasers on the detuning frequency (i.e. effects of laser-wavelength fluctuations). The LS_f points also exhibit reduced disturbances from spontaneous emission noise on the laser field frequency and phase. Consequently, the frequency of the limit cycles at these sensitivity points is still sensitive to the effects of laser-amplitude fluctuations, slave laser bias-current fluctuations, carrier noise, and spontaneous emission noise on the laser field amplitude. The LS_f points are located at a local P1 frequency extremum with respect to the detuning frequency.

To identify the LS_f points, a weak frequency modulation is added to the master laser frequency to mimic fluctuations in the detuning frequency. Figure 3.4 shows the responses of the modulation sidebands around a local minimum of the P1 frequency with respect to f. The detuning frequency is swept from $f = -1$ GHz to $f = 10$ GHz, while the other operational parameters are fixed at $\xi = 0.08$ and $\tilde{J} = 1.222$, creating a P1 frequency that has a local minimum at $f = 4$ GHz as a function of f. Two sharp dips in the responses of the modulation sidebands with respect to the P1-frequency carrier are observed at the local P1 frequency minimum, when a weak frequency modulation to the master laser output is applied at $f_f = 500$ MHz, indicating an LS_f point (solid curves). Similarly, Two sharp dips in the responses of the modulation sidebands with respect to the P1-frequency carrier are observed slightly shifted away from the local P1 frequency minimum with respect to f, when bias current modulation to the slave laser bias current is applied at $f_{\tilde{J}} = 500$ MHz (short dashed curves), indicating an $LS_{\tilde{J}}$ point. The responses of the modulations sidebands show no dips when a weak amplitude modulation to the master laser is applied at $f_\xi = 500$ MHz (long dashed curves). This indicates that at an LS_f only the injection-strength fluctuations and the spontaneous emission noise on the laser field amplitude affects the P1 frequency stability. The reason for the simultaneous existence of an LS_f and an $LS_{\tilde{J}}$ at a P1-frequency minimum with respect to f is that modulation on the bias current induces mainly frequency modulation. Therefore, P1 frequency minima with respect to f have reduced sensitivity to slave laser bias-current fluctuations as well as detuning-frequency fluctuations.

A P1 frequency extremum with respect to f can be found at different combinations of the operational conditions ξ, f, and $\tilde{J}$. Therefore, two-dimensional maps with respect to ξ -f, $\tilde{J}$ - f,

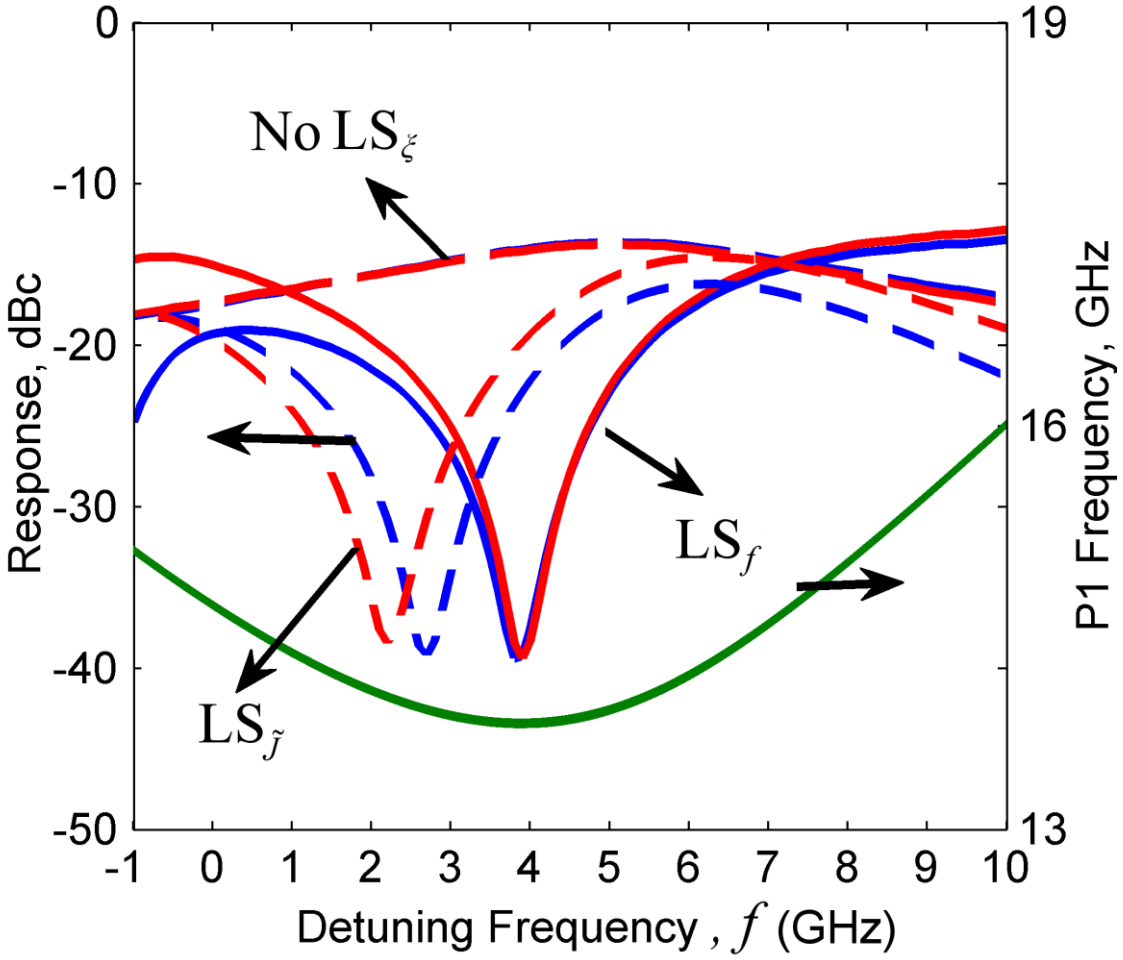

Figure 3.4: Responses of the positive (blue) and negative (red) modulation sidebands of the P1-frequency carrier near a local minimum of P1 frequency (green) with respect to the detuning frequency at fixed ξ = 0.08 and $\tilde{J}$ = 1.222. To identify an LS$_f$ point, a weak detuning-frequency modulation at f_f = 500 MHz is applied (solid curves). To identify an LS$_\xi$ point, a weak injection-strength modulation at f_ξ = 500MHz is applied (long dashed curves). To identify an LS$_{\tilde{J}}$ point, a weak bias-current modulation at $f_{\tilde{J}}$ = 500MHz is applied (short dashed curves).

and ξ - $\tilde{J}$ are calculated to show the LS_f regions. Figures 3.5(a) and (b) show the LS_f regions characterized by suppressed responses of the positive and negative modulation sidebands, respectively, when the bias current is fixed at $\tilde{J}$ = 1.222 while ξ and f are varied. Similar convention used in Figs. 3.3(a) and (b) are used in Figs. 3.5(a) and (b). A large LS_f region is observed close to the Hopf bifurcation curve where the contour curves show P1 frequency minima with respect to the detuning frequency. The LS_f points are characterized by significant suppression of the modulation sidebands. The difference in the responses of the positive and negative modulation sidebands, seen in Figs. 3.5(a) and (b), is attributed to the antiguidence effect characterized by linewidth enhancement factor. The dip in the responses of the modulation sidebands in the power spectrum at an LS point arises from a complex summation involving wave mixing of all of the spectral lines in the optical spectrum [84]. The b factor is responsible for the asymmetry of the optical spectral components, and recent results showed that the region where the responses of the positive and negative modulation sidebands are different consists of highly nonlinear, intensity-asymmetric P1 dynamics [116, 117].

Figures 3.5(c) and (d) show the LS_f regions characterized by suppressed responses of the positive and negative modulation sidebands, respectively, when the detuning frequency is fixed at f = 10 GHz while ξ and $\tilde{J}$ are varied. Similar convention used in Figs. 3.3(c) and (d) are used in Figs. 3.5(c) and (d). Although f is fixed, a large region of LS_f points is observed, indicating P1 frequency minima with respect to f. The P1 frequency minima with respect to f are in the third axis not shown in the two-dimensional maps of Figs. 3.5(c) and (d). These P1 frequency minima happen to be at or close to f = 10 GHz for different combinations of ξ and $\tilde{J}$. The difference in the modulation sidebands in Figs. 3.5(c) and (d) is more prominent close

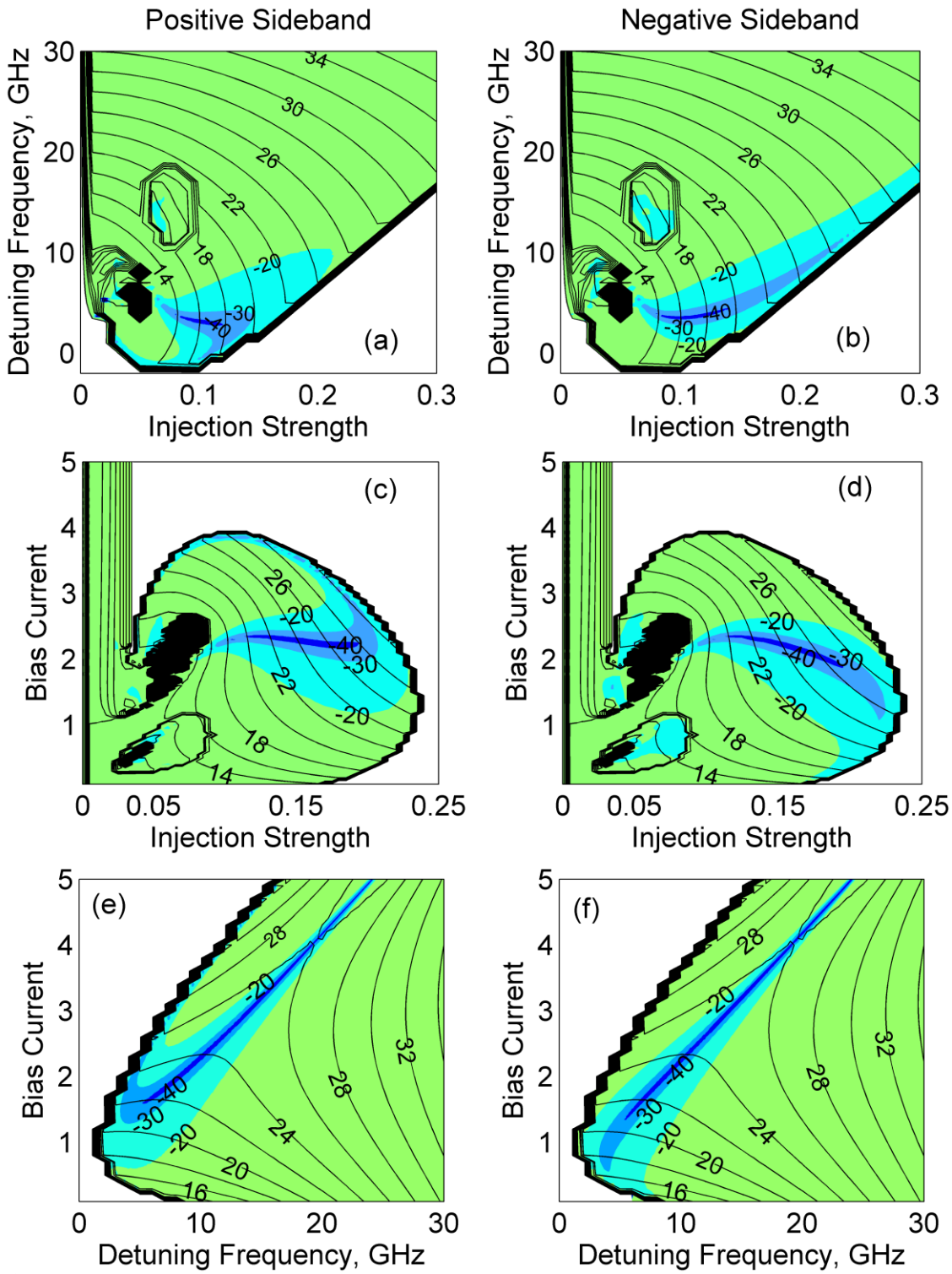

Figure 3.5: Mapping of the LS_f regions obtained by applying a weak modulation on the detuning frequency at f_f = 500 MHz. Similar convention used in Fig. 3.3 is used here.

to the Hopf bifurcation curve, where the highly nonlinear, intensity-asymmetric P1 dynamics are located.

Figures 3.5(e) and (f) show the LS_f regions characterized by suppressed responses of the positive and negative modulation sidebands, respectively, when the injection strength is fixed at ξ = 0.15 while f and $\tilde{J}$ are varied. The Hopf bifurcation curve (thick black curve) separates the stable locking region (uncolored) from the P1 region (colored). The contour curves represent the P1 frequency in GHz. A large LS_f region across the P1 frequency minima is observed, illustrating the tunability of the LS_f points. LS_f points at frequencies up to three times the relaxation resonance frequency of the laser are observed for high bias currents. Figures 3.5(e) and (f) show that narrow or broad dips in the responses of the modulation sidebands with respect to the tuned control parameter, represented by rapidly or gradually decreasing amplitudes of the modulation sidebands, respectively, is associated with the sharpness of the P1 frequency with respect to the tuned control parameter as indicated by the contour curves. Similar to Figs. 3.5(a)-(d), the difference in the modulation sidebands of the P1 frequency is prominent close to the Hopf bifurcation curve, where the highly-nonlinear, intensity-asymmetric P1 dynamics are located.

3.2.3 Low Sensitivity to Bias-Current Fluctuations

P1 oscillations with reduced sensitivity to fluctuations in the slave laser bias current, $LS_{\tilde{J}}$, show reduced sensitivity to fluctuations in the temperature and bias current of the slave laser and the temperature but not the bias current of the master laser [83]. The $LS_{\tilde{J}}$ points also exhibit reduced disturbances from carrier noise on the slave laser. Therefore, the frequency of the limit cycles at these sensitivity points is only sensitive to the effects of laser-amplitude

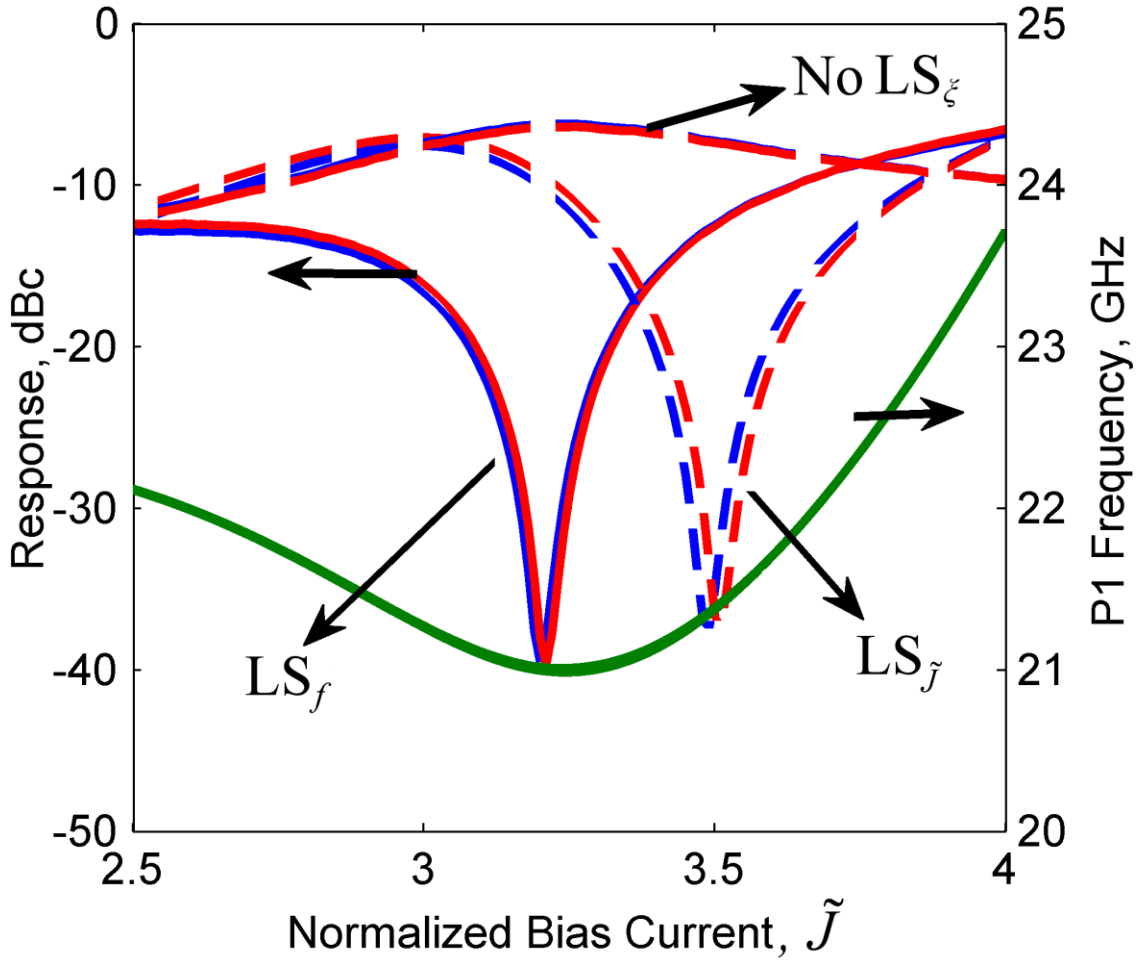

Figure 3.6: Responses of the positive (blue) and negative (red) modulation sidebands of the P1-frequency carrier near a local minimum of P1 frequency (green) with respect to the normalized bias current at fixed f = 15 GHz and ξ = 0.12. To identify an LS$_f$ point, a weak detuning-frequency modulation at f_f = 500 MHz is applied (solid curves). To identify an LS$_\xi$ point, a weak injection-strength modulation at f_ξ = 500MHz is applied (long dashed curves). To identify an LS$_{\tilde{J}}$ point, a weak bias-current modulation at $f_{\tilde{J}}$ = 500MHz is applied (short dashed curves).

fluctuations and spontaneous emission noise on the laser filed amplitude. The $LS_{\tilde{J}}$ points are located at close proximity to a local P1 frequency extremum with respect to $\tilde{J}$ or f.

To identify the $LS_{\tilde{J}}$ points a weak current modulation is added to the slave laser to mimic fluctuations in the bias current. Figure 3.6 shows the responses of the modulation sidebands around a local minimum of the P1 frequency with respect to $\tilde{J}$. The weak current modulation is at $f_{\tilde{J}}$ = 500MHz to simulate current or carrier noise at 500MHz. The bias current is swept from $\tilde{J}$ = 2.5 to $\tilde{J}$ = 4, with the other operational parameters fixed at f = 15 GHz and ξ = 0.12, creating a P1 frequency with a local minimum at $\tilde{J}$ = 3.2 as a function of $\tilde{J}$. Two sharp dips in the responses of the modulation sidebands with respect to the P1-frequency carrier are observed at close proximity, but not exactly at the location, of the local P1 frequency minimum, indicating an $LS_{\tilde{J}}$ point (short dashed curves). Similarly, Two sharp dips in the responses of the modulation sidebands with respect to the P1-frequency carrier are observed at the local P1 frequency minimum with respect to $\tilde{J}$, when detuning-frequency modulation to the master laser frequency is applied at f_f = 500 MHz (solid curves), indicating an LS_f point. The responses of the modulations sidebands show no dips when a weak amplitude modulation to the master laser is applied at f_ξ = 500 MHz (long dashed curves). The reason for the simultaneous existence of an LS_f and an $LS_{\tilde{J}}$ in Fig. 3.6 is that a P1 frequency minimum with respect to f overlaps with the P1 minimum with respect to $\tilde{J}$. Therefore, such simultaneous LS_f and $LS_{\tilde{J}}$ point is qualitatively different than the simultaneous LS_f and $LS_{\tilde{J}}$ points shown in Fig. 3.4. This indicates that at an $LS_{\tilde{J}}$ point the injection-strength fluctuations, detuning-frequency fluctuations, and the spontaneous emission noise affects the P1 frequency stability. Unless a P1 frequency minimum with respect to $\tilde{J}$ overlaps with the P1 frequency minimum with respect to f, as in Fig. 3.6, only injection-strength fluctuations and

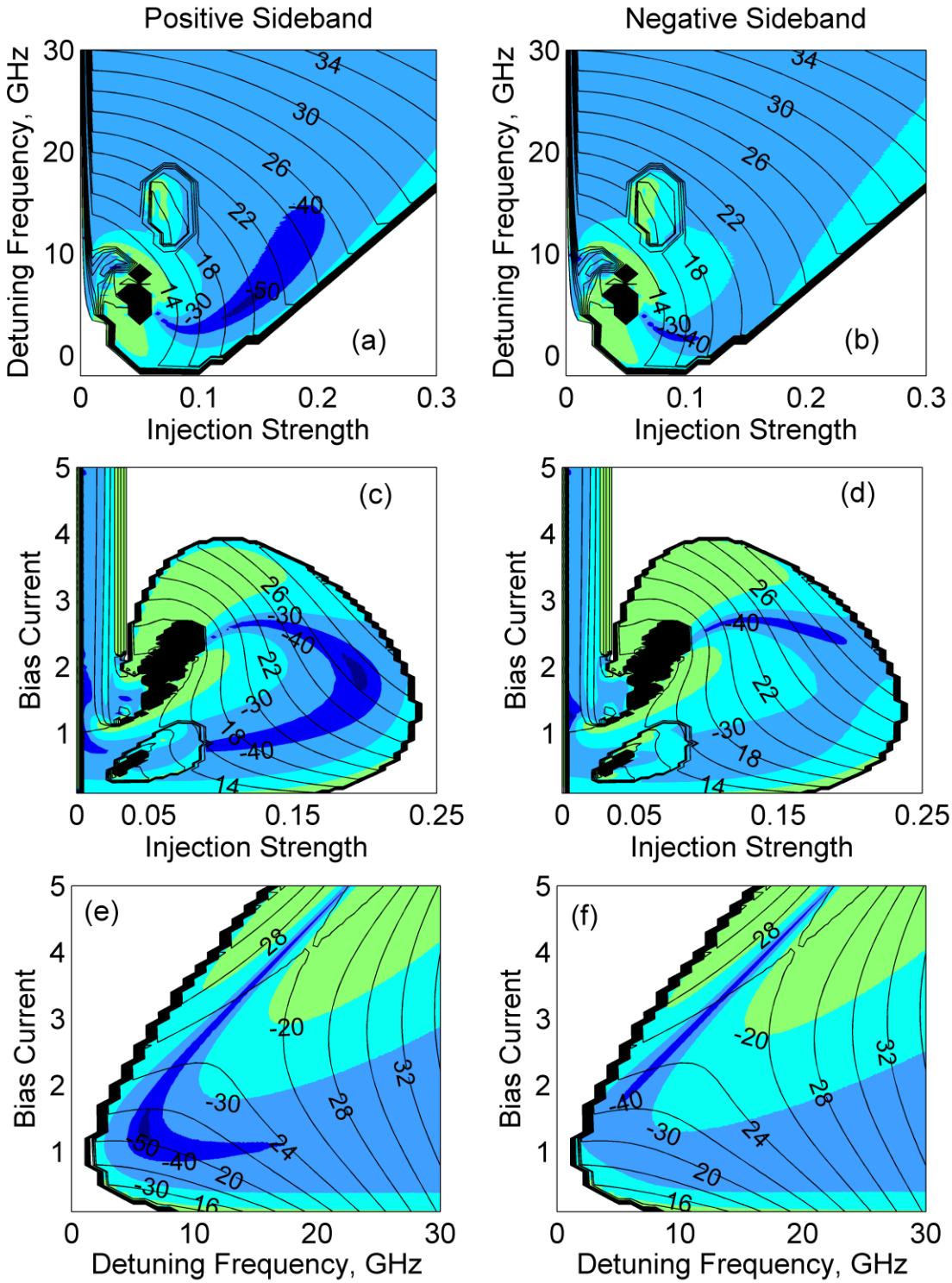

Figure 3.7: Mapping of the LS$_j$ regions obtained by applying a weak current modulation to the slave laser bias current at f_j = 500 MHz. Similar convention used in Figs. 3.3 and 3.5 is used here.

the spontaneous emission noise on the laser field amplitude affects the P1 frequency stability.

A P1 frequency extremum with respect to $\tilde{J}$ can be found at different combinations of the operational conditions ξ, f, and $\tilde{J}$. Therefore, two-dimensional maps with respect to ξ -f, $\tilde{J}$ - f, and ξ - $\tilde{J}$ are calculated to show the $LS_{\tilde{J}}$ regions. Figures 3.7(a) and (b) show the $LS_{\tilde{J}}$ regions characterized by suppressed responses of the positive and negative modulation sidebands, respectively, when the bias current is fixed at $\tilde{J}$ = 1.222 while ξ and f are varied. Although $\tilde{J}$ is fixed, a region of $LS_{\tilde{J}}$ is identified where the P1 frequency is at a minimum with respect to f. The reason as stated above is that, unlike the LS_f points, the $LS_{\tilde{J}}$ points can generally be found both at a P1 frequency extremum with respect to $\tilde{J}$ and at a P1 frequency extremum with respect to f [83]. This stems from the fact that modulation on the bias current of the slave laser induces primarily frequency modulation and therefore creates a modulation on the detuning frequency. By contrast, a modulation on the master laser frequency does not affect the bias current of the slave laser; therefore, an LS_f point is not found at a P1 frequency extremum with respect to $\tilde{J}$. Figures 3.7(c) and (d) show the $LS_{\tilde{J}}$ regions characterized by suppressed responses of the positive and negative modulation sidebands, respectively, when the detuning frequency is fixed at f = 10 GHz while ξ and $\tilde{J}$ are varied. A large region of $LS_{\tilde{J}}$ points originate from two different types of local P1 frequency minima, one with respect to $\tilde{J}$ and the other with respect to f. A comparison between Figs. 3.5(c) and (d) with Figs 3.7(c) and (d) shows that an $LS_{\tilde{J}}$ point that overlaps with an LS_f point originates from a P1 frequency minimum with respect to f, whereas an $LS_{\tilde{J}}$ point that does not overlap with an LS_f point originates from a P1 frequency minimum with respect to $\tilde{J}$.

Figures 3.7(e) and (f) show the $LS_{\tilde{J}}$ regions characterized by suppressed responses of the positive and negative modulation sidebands, respectively, when the injection strength is fixed at ξ = 0.15 while the f and $\tilde{J}$ are varied. A large $LS_{\tilde{J}}$ region is observed but slightly shifted away from the P1 frequency minima. The origin of the $LS_{\tilde{J}}$ can be found when comparing Figs 3.5(e) and (f) to Figs. 3.7(e) and (f): An overlap between LS_f and $LS_{\tilde{J}}$ indicates an $LS_{\tilde{J}}$ point originating from a P1 frequency minimum with respect to f, whereas no overlap between the two indicates an $LS_{\tilde{J}}$ originating from a P1 frequency minimum with respect to $\tilde{J}$. In both cases, an $LS_{\tilde{J}}$ is always slightly shifted away from the P1 frequency minimum. A sharp P1 frequency minimum corresponds to narrow modulation sideband dips in both cases where a P1 minimum is found with respect to f or $\tilde{J}$, whereas a dull P1 frequency minimum corresponds to broad dips, as illustrated by the contour curves. An $LS_{\tilde{J}}$ point associated with a dull P1 frequency extremum is shifted significantly away from the extremum, as illustrated in the bottom part of Figs. 3.7(e) and (d).

3.2.4 Fluctuation-Frequency Dependence of the Low-Sensitivity Points

The mappings of the various LS points illustrated in the preceding sections are all created at a modulation frequency of 500 MHz. In numerical simulations and experimental demonstration, 500 MHz modulation frequency showed easily identified modulation sideband dips to compare theoretical and experimental results. Lower modulation frequencies show much deeper modulation sideband dips. To investigate the dependence of the LS points on the fluctuation frequency, weak modulation with a frequency of 100 MHz to 2 GHz is applied to the each type of LS point. The modulation sideband response varies as the modulation frequency is varied. The dips of the modulation sidebands are compared to the modulation

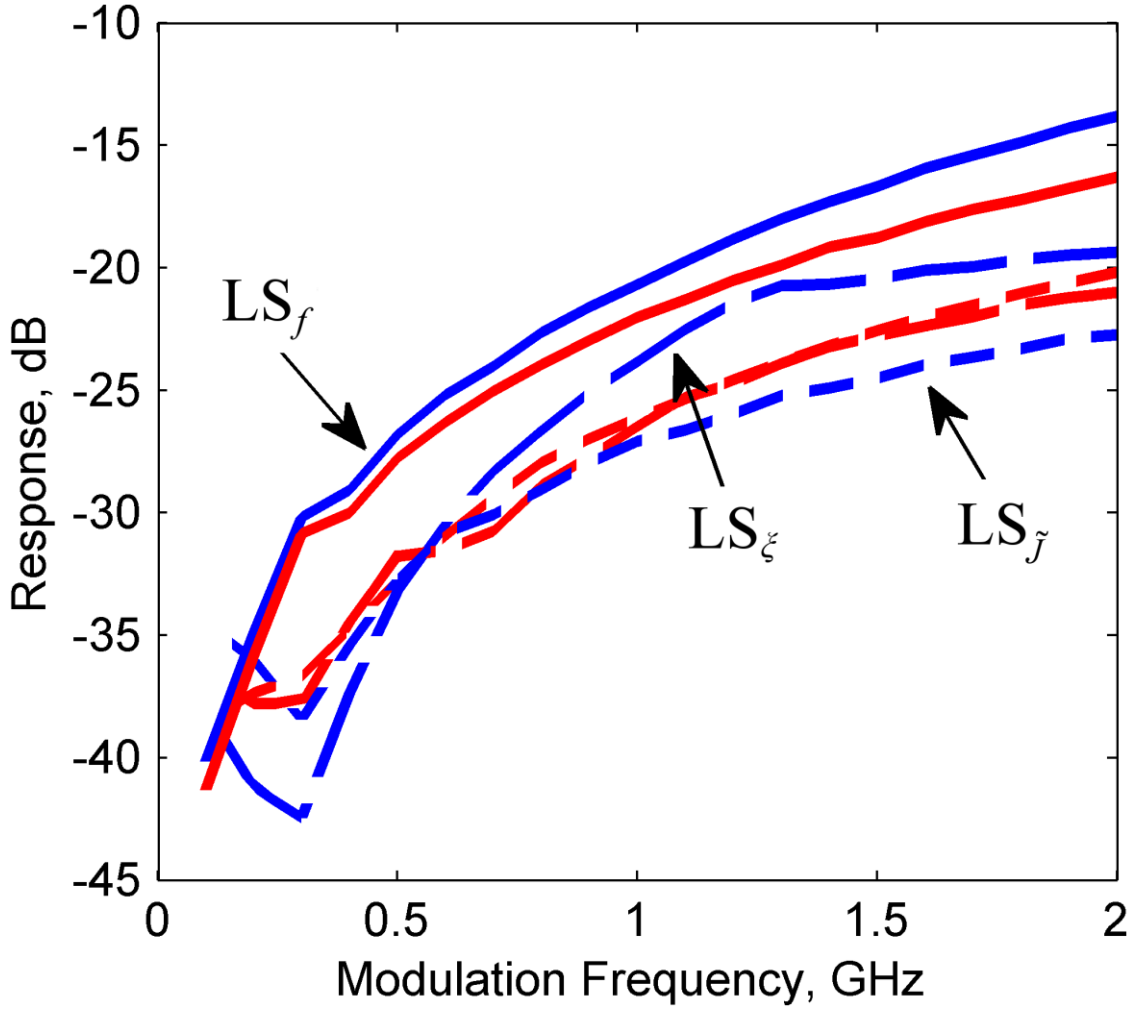

Figure 3.8: Frequency dependence of the positive (blue) and negative (red) modulation sideband dips for an LS$_\xi$ (long dashed curves), LS$_f$ (solid curves) and LS$_{\tilde{J}}$ (short dashed curves) at (ξ, f, $\tilde{J}$) = (0.05-0.08, 10 GHz, 2.8) , (ξ, f, $\tilde{J}$) = (0.08,1-10 GHz, 1.222), and (ξ, f, $\tilde{J}$) = (0.12,15 GHz, 1-4), respectively.

sidebands response further away from the dips to measure the amount of suppression. Figure 3.8 shows the modulation sideband dips of an LS_{ξ} (long-dashed curve), LS_{f} (solid curve) and $LS_{\tilde{J}}$ (short-dashed curve) at (ξ, f, $\tilde{J}$) = (0.05-0.08, 10 GHz, 2.8), (ξ, f, $\tilde{J}$) = (0.08, 1-10 GHz, 1.222), and (ξ, f, $\tilde{J}$) = (0.12, 15 GHz, 1-4), respectively, as a function of the modulation frequency. Because most fluctuations that contribute to the noise of a semiconductor lasers are low-frequency fluctuations, the characteristics seen in Fig. 3.8 demonstrate the effectiveness of the LS points in suppressing the laser noise. Indeed, the stability of the P1 frequency against fluctuations increases significantly with the decrease of the fluctuation frequency for the various types of LS points. As seen in Fig. 3.8, the modulation sideband dips slowly fade away as the modulation frequency is increased to the order of a few GHz. Because the linewidth of the P1 frequency of a semiconductor laser is typically on the order of 100 MHz or tens of MHz, this characteristic allows an LS point to suppress noise caused by broadband intrinsic and extrinsic noise sources.

3.3 Period-Two Low-Sensitivity Points

Period-two dynamics of the optically injected laser are characterized by the emergence of a subharmonic frequency exactly at half the fundamental frequency. They appear when the system undergoes a period-doubling bifurcation as one of the control parameters is tuned [81]. The mappings in Figs. 3.3, 3.5, and 3.7 show two regions of the P2 dynamics encircled by dense curves marking the period-doubling bifurcation. The two P2 regions found in our laser system are both illustrated in Figs. 3.3(a) and (b) and in Figs. 3.3(c) and (d) through different cuts. The frequency bandwidth of an LS point is where the dips in the responses of the modulation sidebands are prominent before fading away as the modulation frequency is

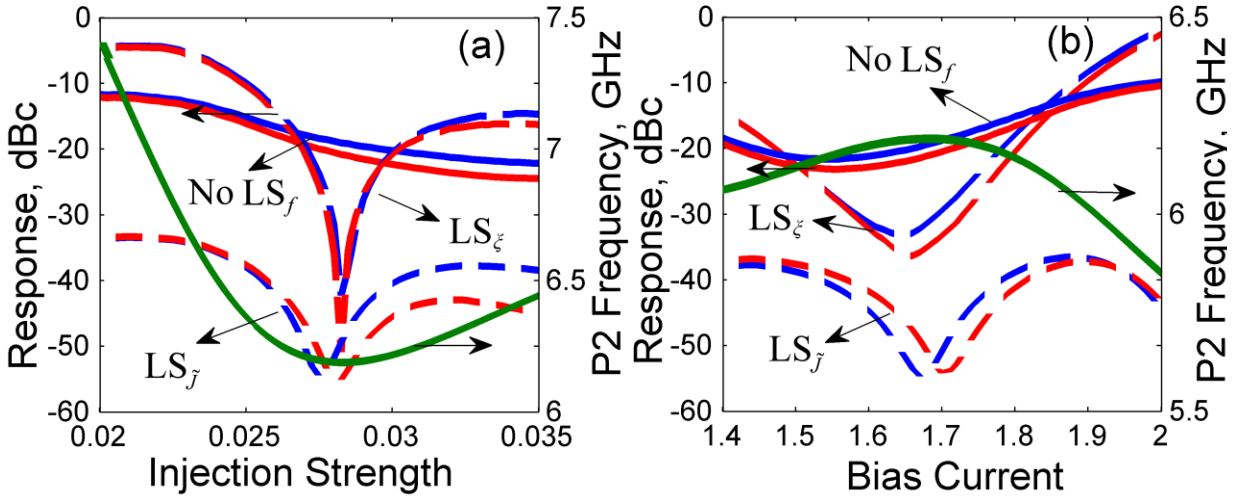

Figure 3.9: Responses of the positive (blue) and negative (red) modulation sidebands of the P2-frequency carrier near a local extremum of P2 frequency (green) with respect to: (a) the injection strength at fixed f = 10 GHz, $\tilde{J}$ = 1.7 and (b) the bias current at fixed ξ = 0.028, f = 10 GHz. To identify an LS$_f$ point, a weak modulation at 100 MHz is applied on the detuning frequency (solid curves). To identify an LS$_\xi$ point, a weak modulation at 100 MHz is applied on the injection strength (long dashed curves). To identify an LS$_{\tilde{J}}$ point, a weak modulation at 100 MHz is applied on the bias current (short dashed curves). For clarity, the LS$_{\tilde{J}}$ modulation response curves are down-shifted by 20dB.

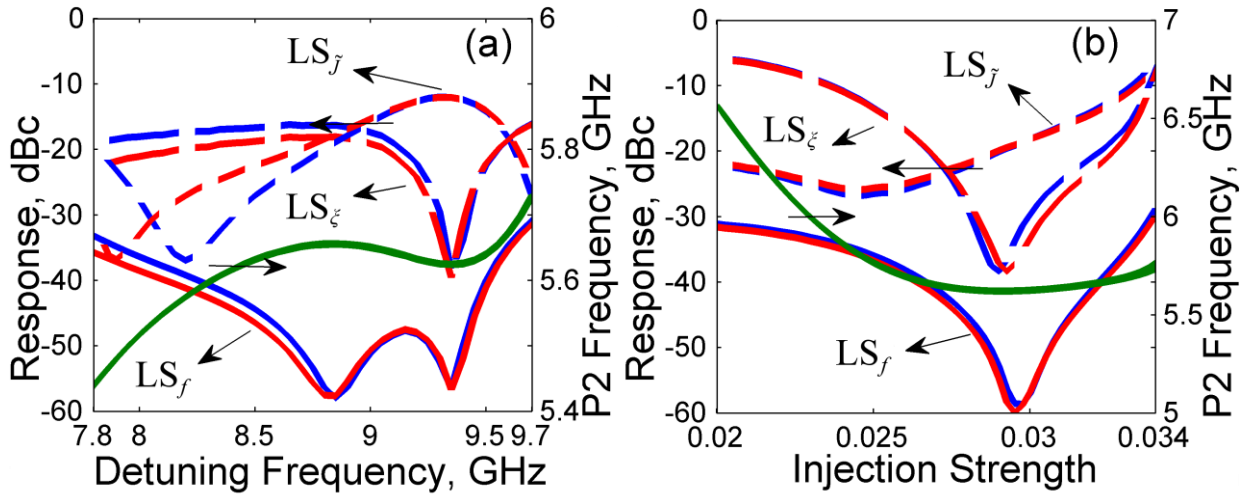

Figure 3.10: Responses of the positive (blue) and negative (red) modulation sidebands of the P2-frequency carrier near a local extremum of P2 frequency (green) with respect to (a) the detuning frequency at fixed $\xi = 0.03$, $\tilde{J} = 1.222$ and (b) the injection strength at fixed $f = 9.3$ GHz, $\tilde{J} = 1.222$. To identify an LS$_f$ point, a weak modulation at 100 MHz is applied on the detuning frequency (solid curves). To identify an LS$_\xi$ point, a weak modulation at 100 MHz is applied on the injection strength (long dashed curves). To identify an LS$_{\tilde{J}}$ point, a weak modulation at 100 MHz is applied on the bias current (short dashed curves). For clarity, the LS$_f$ modulation response curves are down-shifted by 20dB.

increased as illustrated in Fig. 3.8. The bandwidth of an LS point in the P2 dynamic region (LS-P2) is found to be less than that of an LS point in the P1 dynamic region (LS-P1). Therefore, a weak modulation at 100 MHz, instead of 500 MHz, is used to identify LS-P2 points.

Figures 3.9 and 3.10 show the responses of the modulation sidebands when a weak modulation at 100 MHz is applied on the injection strength (long dashed curves), the bias current (short dashed curves), or the detuning frequency (solid curves) to identify an LS_{ξ}-P2, $LS_{\tilde{J}}$-P2, or LS_{f}-P2 point, respectively. Figures 3.9 and 3.10 correspond to the P2 region close to the chaotic region in (a)-(d) of Figs. 3.3, 3.5, and 3.7. Figure 3.9(a) shows the responses of the positive (blue) and negative (red) modulation sidebands around a local minimum of the P2 frequency with respect to ξ for different types of modulation at a modulation frequency of 100 MHz. The injection strength is varied from ξ = 0.02 to 0.035 while the other control parameters are fixed at f = 10 GHz and $\tilde{J}$ = 1.7, showing a local minimum of the P2 frequency at ξ = 0.028. Sharp dips in the responses of the modulation sidebands with respect to the P2-frequency amplitude are observed at the local P2 frequency minimum when a modulation on the injection strength is applied, indicating an LS_{ξ}-P2 point (long dashed curves).

Figure 3.9(b) shows the responses of the positive (blue) and negative (red) modulation sidebands around a local maximum of the P2 frequency with respect to $\tilde{J}$. The bias current is varied from $\tilde{J}$ = 1.4 to 2 while the other operational parameters are fixed at ξ = 0.028 and f = 10 GHz, showing a local maximum of the P2 frequency at $\tilde{J}$ = 1.7. Dips in the responses of the modulation sidebands with respect to the P2-frequency amplitude are observed at the local P2 frequency maximum when a modulation on the bias current is applied, indicating

$LS_{\tilde{J}}$ points (short dashed curves). For clarity, the $LS_{\tilde{J}}$-P2 modulation response curves in Fig. 3.9 are down-shifted by 20dB

Figure 3.10(a) shows the responses of the positive (blue) and negative (red) modulation sidebands around a local minimum and a local maximum of the P2 frequency with respect to f. The detuning frequency is swept from f = 7.8 GHz to 9.7 GHz while the other operational parameters are fixed at ξ = 0.03 and $\tilde{J}$ = 1.222, showing a local maximum of the P2 frequency at f = 8.8 GHz and a local minimum at f = 9.3 GHz. Two dips in the responses of the modulation sidebands with respect to the P2-frequency amplitude are observed at the local P2 frequency extrema, indicating two LS_f points (solid curves). For clarity, the LS_f-P2 modulation response curves in Fig. 3.10 are down-shifted by 20dB.

Figure 3.10(b) shows the responses of the positive (blue) and negative (red) modulation sidebands around a local minimum of the P2 frequency with respect to ξ. The injection strength is varied from ξ = 0.02 to 0.034 while the other control parameters are fixed at f = 9.3 GHz and $\tilde{J}$ = 1.222, showing a local minimum of the P2 frequency at ξ = 0.03.

Similar to the LS points found in the P1 region, Figs. 3.9 and 3.10 show all three distinct LS points in the P2 region. The amplitude of the fundamental frequency is significantly larger than that of the subharmonic in the P2 dynamic; therefore, in the maps of Figs. 3.3, 3.5, and 3.7 the LS-P2 points appear less prominent than the LS points of the P1 dynamics. The responses of the modulation sidebands around the fundamental frequency in the P2 dynamic also dip in a fashion similar to the responses of the modulation sidebands around the subharmonic frequency seen in Figs 3.9 and 3.10.

3.4 Optimal Operating Points

Changes in the bias current and the temperature of a semiconductor laser affect both its oscillating wavelength and output power. Hence, in an optical injection system, fluctuations in the operating temperatures and bias currents of the master and slave lasers affect both the detuning frequency and the injection strength. A particular LS point, therefore, mitigates only the effects of temperature and bias-current fluctuations on the master and slave laser power, such as in the LS_{ξ} case; or only the effects of temperature and bias-current fluctuations on the master and slave laser wavelengths, such as in the LS_{f} case; or only the effect of the bias-current fluctuations of the slave laser, such as in the $LS_{\tilde{J}}$ case. Clearly, it is desirable to have LS points that can simultaneously mitigate the effects of the fluctuations in two or more control parameters. Previously we showed $LS_{f\tilde{J}}$ points that are insensitive to fluctuations in both the detuning frequency and the bias current at a P1 frequency extremum with respect to f [25]. These $LS_{f\tilde{J}}$ points can be found by comparing Figs. 3.5(a)-(f) and 3.7(a)-(f) where an LS_{f} point and an $LS_{\tilde{J}}$ point simultaneously exist at the same location.

For an LS point that makes the P1 frequency simultaneously insensitive to fluctuations in the injection strength and the bias current, a P1 or P2 extremum with respect to the injection strength has to overlap that with respect to the bias current. Figure 3.9 shows such a case where a P2 minimum with respect to ξ, in Fig. 3.9(a), and P2 maximum with respect $\tilde{J}$, in Fig. 3.9(b), overlap while f is fixed at 10 GHz. The responses of the modulation sidebands for a modulation on the injection strength (long dashed curves) and those for a modulation on the bias current (short dashed curves) have dips at the same location due to a minimum of the P2 frequency with respect to ξ and a maximum with respect to $\tilde{J}$. No dips in the modulation sidebands are seen when a modulation on the detuning frequency is applied (solid

curves). Thus, this LS point is a simultaneous $LS_{\xi\tilde{J}}$ point but not an LS_f point. The $LS_{\xi\tilde{J}}$ point can simultaneously suppress the effects of the power fluctuations caused by the fluctuations in the temperatures and bias currents of the two lasers, as well as the effects of the wavelength fluctuations caused by the fluctuations in the temperature and bias current of the slave laser but not the master laser.

For an LS point that is simultaneously insensitive to fluctuation in the injection strength and the detuning frequency, a P1 or P2 extremum with respect to the injection strength has to overlap that with respect to the detuning frequency. Figure 3.10 shows such a case where the minima of the P2 frequency with respect to ξ, shown in Fig. 3.10(a), and f, shown in Fig. 3.10(b), overlap while $\tilde{J}$ is fixed at 1.222. The responses of the modulation sidebands for a modulation on the injection strength (long dashed curves) and those for a modulation on the detuning frequency (solid curves) have dips at the same location. A dip in the responses of the modulation sidebands are seen when a modulation on the bias current is applied (dashed curves) but are shifted significantly away from the P2 minimum into more advanced dynamics (not shown). An $LS_{\xi f}$ point can simultaneously suppress the effects of the wavelength and power fluctuations caused by the fluctuations in the temperatures and bias currents of the two lasers. Due to the effects of the bias-current fluctuations on the detuning frequency, as explained above, an $LS_{\xi f}$ point can be considered insensitive to all three control parameters and therefore an optimal operating point. The P2 oscillation frequency is at a minimum with a frequency of 5.6 GHz at the $LS_{\xi f}$ point shown in Fig. 3.10. Tuning one of the operational parameters will move the P2 oscillation frequency away from its minimum with respect to the injection strength and the minimum with respect to the detuning frequency.

Therefore, the tuning range is restricted by both the injection strength and detuning frequency limiting the oscillation frequency tunability to around 5 GHz to 7 GHz.

In this study, simultaneous low-sensitivity points of the $LS_{\xi J}$ and $LS_{\xi f}$ types are found in the P2 dynamics region but not in the P1 region. The modulation sidebands around the fundamental frequency in the P2 dynamics undergo similar dips as the ones illustrated in Figs. 3.9 and 3.10. The existence and locations of the LS points depend on the intrinsic parameters of the slave laser because these parameters significantly affect the nonlinear dynamics induced by optical injection [26, 29]. For a slave laser that has a set of intrinsic parameters different from those used in this study, optimal operating points of the $LS_{\xi f}$ type might be also found in the P1dynamic region.

3.5 Experimental Results

To verify the numerical calculations discussed above, experiments are performed. The optical injection setup shown in Fig. 2.1 is operated in the P1 dynamic region. Both lasers are temperature and current stabilized as discussed in Chapter 2. To vary the injection strength the variable attenuator or the first HWP is tuned. To vary the detuning frequency the master laser temperature is adjusted for gross frequency changes and then the current was adjusted for fine-tuning of the detuning frequency. The slave laser bias current is fixed at 40 mA for a normalized bias current of $\tilde{J}$ = 1.222, similar to the bias current used in our simulation results. weak current modulation is applied to the slave laser through a bias-tee from the microwave synthesizer at $f_{\tilde{J}}$ = 500 MHz. Figure 3.11 shows the experimentally found LS_J point at a P1 frequency minimum with respect to f. The detuning frequency is

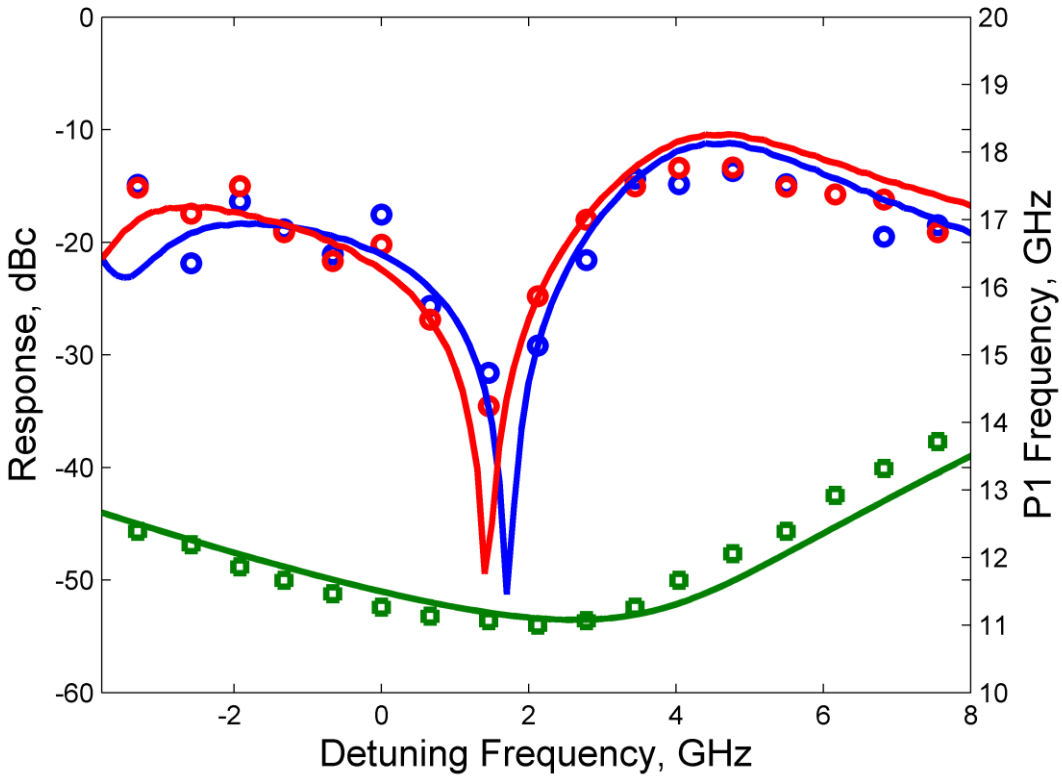

Figure 3.11: Experimentally measured (symbols) and calculated (solid curves) values of the modulation sideband amplitude and the P1 frequency using a normalized injection amplitude of 0.07, a bias current of 40 mA, and a modulation frequency of 500 MHz. This figure shows the positive frequency detuning sideband (blue circles), the negative detuning sideband (red circles), and the corresponding P1 frequency (green squares).

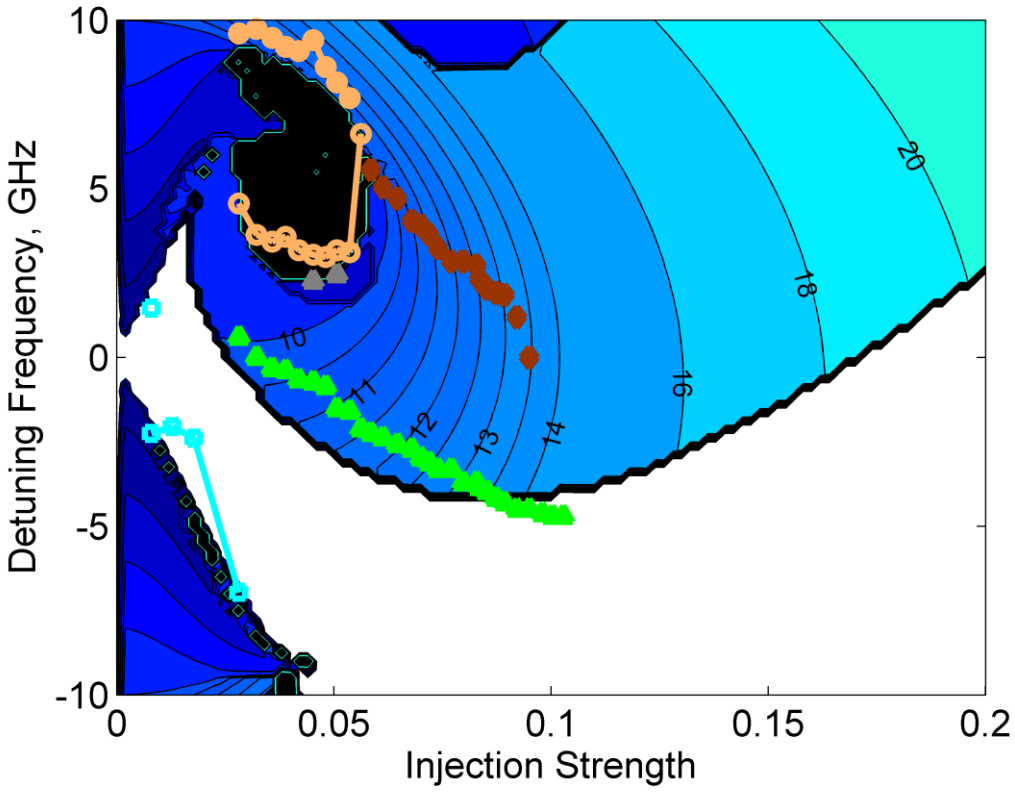

Figure 3.12: Experimentally measured (symbols) and calculated (solid curves) mappings of key transitions in the optical injection laser system as a function of the injection strength and the detuning frequency. Experimental Data—the open squares are the saddle-node bifurcation points that, along with the green triangles representing Hopf Bifurcation points, bound the region of stable locking. The red diamonds mark operating points with a local P1 minimum frequency. The gray triangles mark the P2 Dynamics. The orange circles denote a saddle-node bifurcation of limit cycles, and the open orange circles, mark alternate routes from P1 to more complex dynamics.

swept from $f = -1$ GHz to $f = 8$ GHz by varying the master laser temperature. The injection strength is held constant at a normalized injection strength of $\xi = 0.07$. Dips in the responses of the positive (blue circles) and negative (red circles) modulation sidebands are observed at close proximity to the P1 frequency minimum (green squares) at $f = 2.12$ GHz. The error for the experimentally measured detuning is ± 200 MHz while the depths of the minima were limited by the background noise levels. Similar to the numerical calculations the response of the modulation sidebands are normalized to the P1 frequency amplitude as illustrated in Fig. 3.1.

Figure 3.12 shows the experimental mapping of the key features of the dynamics map of the optically injected semiconductor laser overlapped with the numerical calculations using the model described in Chapter 2. The experimental mapping is created by monitoring the power and optical spectra of the optically injected laser by adding or removing the beam blocker in front of the probe laser, respectively. The saddle-node (blue squares) and the Hopf (green triangles) bifurcations bound the region of stable locking. Chaotic dynamics are bounded by different routes to chaos, from below period-doubling bifurcation (gray triangles) and from above saddle-node of limit cycles (orange circles). The LS_J points (red diamonds) are found at the numerically calculated P1 frequency minima indicated by the contour curves.

The curve of measured and modeled operating points in Fig. 3.12 where the P1 frequency is minimized, the laser switches from a limit cycle where the injected-shifted laser oscillation frequency is pushed away from the injection frequency at larger detuning to a limit cycle where the oscillation frequency is pulled towards the injection frequency for smaller detuning. This change in relative behavior of the system resonance relative to the injection

frequency is necessary, though at higher injection levels we observe a smooth rather than abrupt transition. Frequency pushing behavior arises from the fact that the semiconductor laser is a detuned oscillator, while the frequency pulling behavior is the kind expected from an Adler-type analysis of an injected oscillator. A local minimum of the P1 frequency is where these two opposing effects balance out.

To get quantitative comparisons of theory and experiment as shown in Figs. 3.11 and 3.12 the laser intrinsic parameters were adjusted within their experimentally defined error margins. The measured relaxation rates have ± 10% error while the b and b' have ± 15% and ± 50%, respectively. A more detailed description of the adjusted parameters will be discussed in Chapter 4. Since the actual power injected into the slave laser is difficult to determine, the injection strength is used as our only fitting parameter. Nevertheless, it is determined by fitting the negative offset saddle-node bifurcation experimental data to the model calculations. This then fully determines the experimental map and the agreement is excellent. Further, the agreement between data and model in Fig. 3.11 shows that even detailed features of the system can be fully recovered in quantitative agreement. This degree of accuracy requires careful determination of the dynamic parameters that go into the model. As discussed in the previous chapter, the intrinsic parameters are experimentally determined using a well-established four wave mixing technique.

The gain saturation factor was introduced to account for the offsets of the response of the modulation sideband dips to the P1 frequency minima. Note that the saturation effects do not need to be included in the model to observe the reduced sensitivity points. Suppressing the nonlinear gain ($\gamma_p = 0$, $b' = 0$) still maintains the LS points but at significantly shifted injection strength and frequency detuning. Therefore, nonlinear gain effects such as spectral hole

burning or carrier heating do not determine the LS points. It is the interband carrier dynamics, and their effects on the refractive index of the gain medium, that principally determine when the wave mixing of the various optical frequency components will lead to destructive interference and the minimization of sensitivity to perturbations. Saturation effects and nonlinear gain effects in general, however, do play a key role in the relative positioning of the sensitivity minima with respect to the various bifurcations in the mapping and will be discussed in Chapter 4.

3.6 Summary

In summary, we showed that the nonlinearities of the optical injection system can be used to stabilize the photonic microwave frequency generated by limit-cycle oscillations at specific operating points. These LS operating points are found at the local extrema of the P1or P2 frequency with respect to one or more of the control parameters.

Two-dimensional mappings as functions of different sets of control parameters show regions where different types of LS points exist. An LS_{ξ} point is found at an extremum of the P1 frequency with respect to ξ in a region bounded by the Hopf bifurcation curve and a chaos region. These points show reduced sensitivity to the effects of the fluctuations in the temperatures and bias currents of the lasers on the injection strength, along with reduced effects from spontaneous emission noise on the laser field amplitude. An LS_f point is found at an extremum of the P1 frequency with respect to f in a region close to the Hopf bifurcation curve. These points show reduced sensitivity to the effects of the fluctuations in the temperatures or bias currents of the lasers on the detuning frequency, along with reduced effects from spontaneous emission noise on the laser field frequency and phase. An LS_j point is

found at an extremum of the P1 frequency with respect to $\tilde{J}$ and/or f in a region close to the Hopf bifurcation curve. These points show reduced sensitivity to the fluctuations in the temperatures or bias currents of the slave laser and in the temperature but not the bias current of the master laser, along with reduced effects from carrier noise on the slave laser and spontaneous emission noise on the laser field frequency and phase. Each $LS_{\tilde{J}}$ point is found at a P1 frequency extremum with respect to $\tilde{J}$ and/or f because a modulation on the bias current of the slave laser induces detuning-frequency modulation as well. On the other hand, an LS_f point cannot be found at a P1 frequency extremum with respect to $\tilde{J}$, unless it happens to overlap with a P1 frequency extremum with respect to f, because a modulation on the detuning frequency does not affect the bias current of the slave laser. Both LS_f and $LS_{\tilde{J}}$ points can be found at frequencies up to three times the relaxation resonance frequency of the slave laser by tuning the bias current.

Operating points that have reduced sensitivity to fluctuations in two or more control parameters are found in the P2 dynamics region. These points exist due to a P2 frequency having an extremum with respect to two control parameters simultaneously. At an $LS_{\xi\tilde{J}}$ point, the P2 frequency has reduced sensitivity to fluctuations in the injection strength and in the bias current. At an $LS_{\xi f}$ point, the P1 frequency has reduced sensitivity to fluctuations in the injection strength and the in detuning frequency. Fluctuations in the bias current can also be suppressed at an $LS_{\xi f}$ point since fluctuations in the bias current leads primarily to detuning-frequency fluctuations. Therefore, $LS_{\xi f}$ points can be considered as optimal operating points. Finally, an experimental verification of the LS points and mapping of the key features of the dynamics map showed excellent quantitative agreement between theory and experiment. Note that the laser used in this work has a low relaxation resonance frequency of 10.25 GHz

and reaches an LS point with a P1 oscillation frequency of 30 GHz. For a high-speed laser with a higher relaxation resonance frequency having a modulation bandwidth of 30 GHz, the optically injected laser can reach an LS point with P1 oscillation frequencies of 90 GHz or higher. Furthermore, the P1 & P2 oscillations induced by optical injection discussed in this work are generated through an all-optical system without the need of an external modulation source, which is required in the case of a directly modulated laser.

CHAPTER 4

Controlling the Gain Saturation Factor for Stable Photonic Microwave Generation

This chapter investigates the effects of the intrinsic parameters of the semiconductor laser on the nonlinear dynamics induced by optical injection. The effects of the gain saturation factor on the characteristics of the nonlinear phenomena are studied to find the optimal operating conditions for various application requirements. Such requirements include high microwave frequency, broadband frequency tunability, high modulation bandwidth, optical single-sideband modulation, low phase noise, and stability. The characteristics of optically injected semiconductor lasers with different *b'* factors are compared and analyzed.

4.1 Introduction

The effects of the intrinsic laser parameters on the optically injected laser have been previously investigated [115]. The linewidth enhancement factor, *b*, also known as the antiguidance factor, is a representation of the coupling between the amplitude and phase of the intracavity laser field. It is the ratio of the carrier-induced variations of the real and imaginary parts of the complex susceptibility. This factor is responsible for the rich dynamics in semiconductor lasers [115]. The effects of *b* on the P1 dynamics of an optically injected laser indicate a strong relation between the emergence of the P1 dynamics and the preferred cavity resonance under external perturbation; a large value of *b* favors the occurrence of the P1 dynamics [118]. By contrast, the gain saturation factor, *b'*, is the ratio of the photon-

induced variations of the real and imaginary parts of the complex susceptibility [119]. When studying the nonlinear dynamics of semiconductor lasers, the role of b' is usually neglected by assuming it to be equal to either b or zero. The spectral asymmetry of a weakly modulated semiconductor laser is used to determine the values of b and b' of the laser [119]. It shows that the assumption of either $b = b'$ or $b' = 0$ is not necessarily accurate; while b is generally positive, b' can have a positive [119] or negative [44] value that is different from b. The b and b' factors affect the characteristics of any semiconductor laser system that has phase-sensitive dynamics, such as a laser subject to optical injection or optical feedback. The relaxation rates γ_p and γ_n both vary linearly with $\tilde{J}$ and have opposing effects on the laser dynamics. It has been shown that γ_p has a suppressing effect to the instability of the perturbed laser, whereas γ_n has a supporting effect to the instability of the perturbed laser [115].

4.2 Gain Saturation Factor Experimental Measurement.

Similar to how the b factor was introduced for semiconductor lasers to account for the enhancement of the linewidth of the laser beyond the Schalow-Townes limit [120], the b' factor is introduced to account for the asymmetry in the optical spectrum of the current modulated laser [84]. Although b' is usually neglected in many works involving semiconductor laser modeling, it proves to be essential when quantitative fitting of the experimental data is desired [114, 121]. The excellent quantitative fitting of the experimental data done in Section (3.5) can be achieved only when introducing b' in the theoretical model. Note that because γ_c is approximately two orders of magnitude larger than the other rates, the relaxation resonance frequency is typically much larger than the damping rate and is only weakly dependent on the nonlinear gain relaxation rate. Because of this, one can get good semi-

quantitative agreement between model and experiment even with $\gamma_p = 0$, or equivalently $\partial g/\partial|A|^2 = 0$. As a consequence, all of the key experimentally measured features of the optically injected semiconductor laser discussed in this work can be reproduced with $\gamma_p = 0$ (and a modified value of b and other relaxation rates), but at significantly offset values of the detuning frequency and injection parameter relative to the experimentally measured values.

Many experimental techniques have been developed to measure b and b' [121]. Since the intrinsic parameters of the laser used in this work have been previously measured [15], we use a technique that uses the spectral characteristics of the laser under weak current modulation to measure b' [119]. The technique relies on the frequency dependence asymmetry of the modulation sidebands. Turning off the master laser and using the LO laser for heterodyne detection, the modulation sidebands of the current modulated slave laser are measured at different modulation frequencies. The ratio of the positive to the negative modulation sidebands for different bias currents is shown in Fig 4.1. To extract the b and b' from the experimental measurements it is fitted against the modulation sideband equation [119]:

$$\frac{\left|A_{\pm\tilde{J}}\right|^2}{\left|A_0\right|^2} = \frac{\left\{\left[1 \pm (b-b')\frac{\gamma_p}{\Omega_{\tilde{J}}}\right]^2 + b^2\right\}}{(-\Omega_{\tilde{J}}^2 + \Omega_r^2)^2 + \Omega_{\tilde{J}}^2\,\gamma_r^2} \frac{\gamma_c^2\gamma_n^2}{4} \frac{(\tilde{J}+1)^2}{\tilde{J}^2} m_{\tilde{J}}^2 \qquad (4.1)$$

where $A_{\pm\tilde{J}}$ is the amplitude of the positive and negative modulation sidebands, respectively. Equation (4.1) is derived by perturbation analysis of the directly modulated rate equations shown in equations (2.5)-(2.7) and represents the positive or negative modulation sideband normalized to the central peak [42, 119]. The term $(b-b')\frac{\gamma_p}{\Omega_{\tilde{J}}}$ represents the asymmetry in the optical spectrum and shows symmetric sidebands when $b = b'$. Equation (4.1) also shows

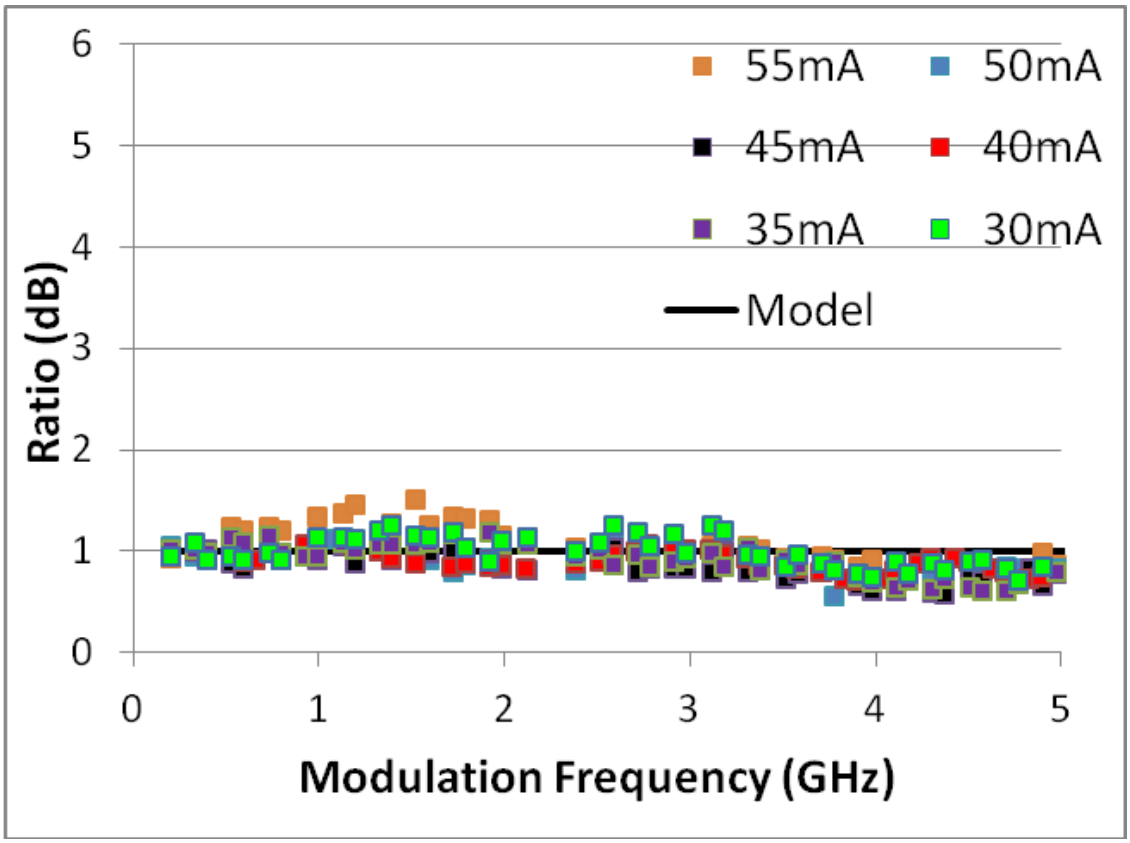

Figure 4.1: Asymmetry of the modulation sidebands given as the ratio of the positive to negative sidebands as the modulation frequency is varied. The modulation sidebands are measured at different bias currents from 30 mA to 55 mA at 5-mA increments. Experimental data are shown as colored squares. The calculated curve using Eq. (4.1) in black gives a value of $b \approx 3.2$ and $b' \approx 3.2$ to fit the experimental data.

Table 4.1

Values for the model parameters and their associated experimental uncertainty

Parameters	Experimental Values	Error Margins	Adjusted Values	% Difference
b	3.2	± 15 %	3.3	3.125
b'	3.2	± 50 %	1.6	-50
γ_c	5.36×10^{11}	± 10 %	5.0×10^{11}	-6.72
γ_s	5.96×10^{9}	± 10 %	5.96×10^{9}	0
γ_n	$6.16 \cdot \tilde{J} \times 10^{9}$	± 10 %	$5.73 \cdot \tilde{J} \times 10^{9}$	-7.04
γ_p	$1.56 \cdot \tilde{J} \times 10^{10}$	± 10 %	$1.41 \cdot \tilde{J} \times 10^{10}$	-9.78

that for $b \neq b'$ the modulation sideband ratio will have a maximum that depends on the value b only, while its offset frequency will depend on b' and γ_p. From Fig. 4.1 the ratio of the positive to negative modulation sidebands is constant as the modulation frequency is tuned from 0 GHz to 5 GHz indicating that b is equal to b' with a value of 3.2 which was previously measured [15]. Since the b' factor represents the ratio of the photon-induced variations of the real and imaginary parts of the complex susceptibility, a study of the effects of the bias current on b' is warranted. This is also demonstrated in Fig. 4.1, as the bias-current is increased from 30 mA to 55 mA no change in the dependence of the modulation sideband ratio on the frequency is observed, indicating that b' is constant as the bias current is increased for the laser used in this work. Although the measurements here show the value of b' to be equal to b at 3.2, using these values to fit the experimental measurements done in Chapter 3 does not show good agreement. Therefore, the value of b' has been tuned to a value of 1.6 along with other adjustments to the relaxation rates to get a better fit. Table 4.1 shows the original values of the intrinsic parameters measured through the techniques mentioned above and their

adjusted values used in the theoretical modelto fit the experimental data. The reason for such large discrepancy in the b' value comes from the accuracy of the measurement technique used here which is ± 15 % accuracy for b and ± 50 % accuracy for b' [44]. All the relaxation rates are adjusted within their error margins of ± 10 %, which is determined by the accuracy of the FWM experimental technique used to extract them.

4.3 Effects on Stable-Locking Dynamics

Stable optical injection leads to significant changes in the modulation characteristics of a semiconductor laser. An increase in the modulation bandwidth and relaxation resonance frequency of more than three times their free-running counterparts was reported [15]. The variation in the gain saturation factor b' for different lasers notably affects these characteristics. The variation of b' in DFB lasers depends on whether the DFB laser operates on the red or the blue side of the gain peak [122]. Operating on the red side of the gain peak yields a positive b' factor, while operating on the blue side of the gain peak yields a negative b' factor. The disparity between the positive and negative gain saturation factors is apparent in their influence on the relaxation resonance frequency, modulation bandwidth, and sideband rejection ratio (SRR) on an optically injected laser. Figure 4.2 shows the dynamics maps for four different values of b' while the bias current $\tilde{J} = 1.222$ and other intrinsic laser parameters are held constant. The dynamics maps are simulated by varying the detuning frequency, f, from −20 to 60 GHz and the injection strength, ξ, from 0 to 0.35. Similar convention used in the mappings of Chapter 3 is used here with the contour curves below the Hopf bifurcation line in the uncolored stable locking region signify the peak frequency, f_{pk}, of the modulation response spectrum.

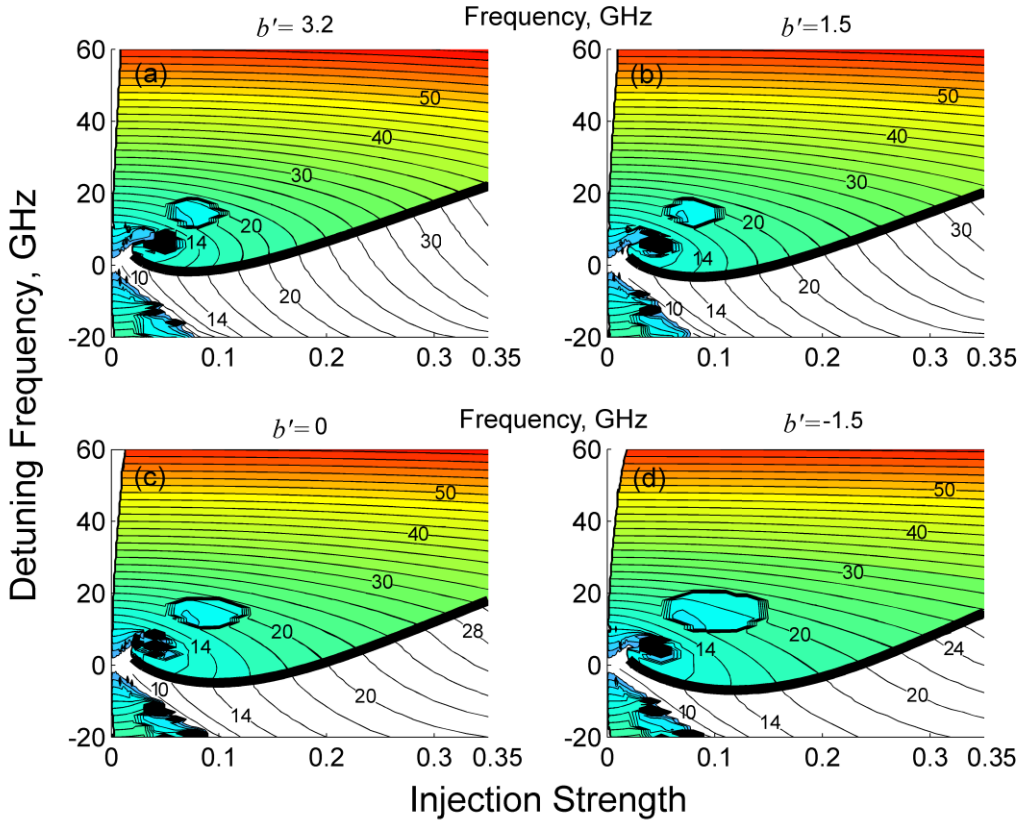

Figure 4.2: Frequency maps, as functions of the optical injection strength and detuning frequency at $\tilde{J}$ = 1.222. The contour curves represent a constant P1 frequency, in GHz, (colored regions) and a constant f_{pk}, in GHz, (uncolored regions). The thick curve represents the Hopf bifurcation line. The second dense curve represents the period-doubling bifurcation. Black regions indicate chaos. The gain saturation factor is varied with (a) $b' = b = 3.2$, (b) $b' = 1.5$, (c) $b' = 0$ and (d) $b' = -1.5$ while the other laser parameters are held constant.

The modulation response spectrum of the slave laser in the stable locking region is calculated by numerically solving the rate equation model in equations (2.5)-(2.7) for a broad range of modulation frequencies. The value of f_{pk} at a given operating point is found by identifying the peak of the modulation response spectrum, and the contour curves in Fig. 4.2 are obtained by varying the detuning frequency and the injection strength for different operating points. Note that f_{pk} is not exactly the same as, but is generally slightly less than, the relaxation resonance frequency, f_r, of the laser because of the finite value of the relaxation rate γ_r [7]. As the b' factor decreases from a value equal to b the instability region increases, showing the lowest point of the Hopf bifurcation line in the map pushed to −7 GHz for $b' = -1.5$ in Fig. 4.2(d) from −1 GHz for $b' = b = 3.2$ in Fig. 4.2(a). The increase in instability is attributed to a reduction in the damping of the relaxation oscillation which is caused by reduced influence of the nonlinear relaxation rate γ_p on the damping as a consequence of the reduction in b'. The nonlinear relaxation rate represents the effect of the nonlinear gain on the system, which is generally believed to result from spectral hole burning in the gain curve [123]. Therefore, the occurrence of the P1 dynamics of an optically injected semiconductor laser favors a smaller or more negative b', which is opposite to the effect b has on the P1 dynamics. In the stable locking region, f_{pk} increases monotonically with the injection strength and with the detuning frequency. Under the same operating condition, f_{pk} increases with b' as illustrated in Fig. 4.3. The injection strength is held constant at 0.4 while the detuning frequency is varied from −5 GHz to −20 GHz at 5-GHz increments, with a more negative detuning frequency showing a lower modulation resonance peak. Different values of b' are represented by colors, with $b' = 3.2$, 1.5, 0 and −1.5 in red, blue, black, and green, respectively. For comparison, the modulation response of the free-running laser is shown in gray.

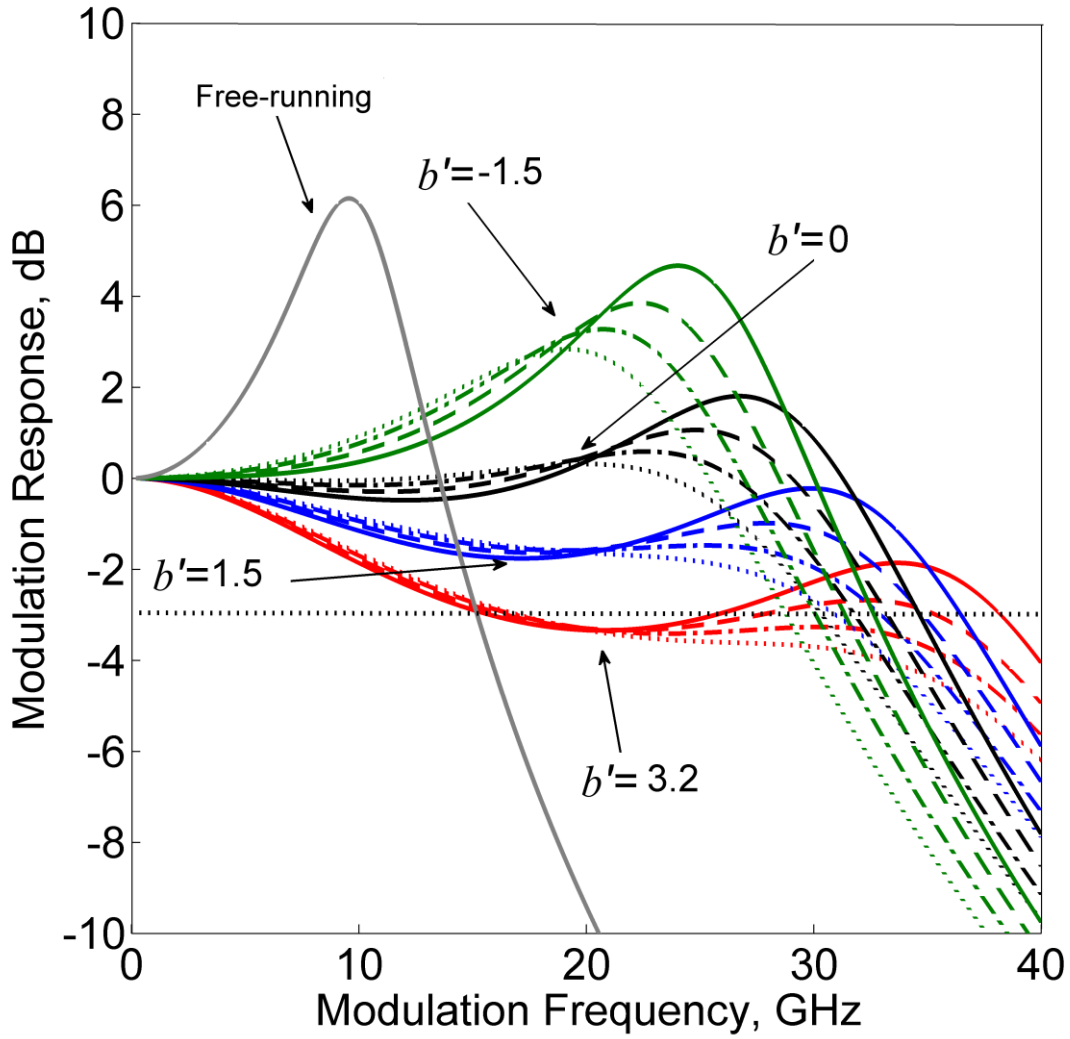

Figure 4.3: The modulation response at a constant injection strength of ξ =0.4 for detuning frequencies of $f = -5$ GHz (solid), $f = -10$ GHz (dash), $f = -15$ GHz (dash-dot) and $f = -20$ GHz (dotted). The colors represent the value of the gain saturation factor $b' = 3.2$ (red), $b' = 1.5$ (blue) $b' = 0$ (black) and $b' = -1.5$ (green). The free-running modulation response (gray) shows a modulation bandwidth of 15GHz. The horizontal dotted line is at −3 dB.

By comparing Fig. 4.2(a) and (d) or comparing the red and green curves of Fig. 4.3, it is seen that the value of f_{pk} for a laser with $b' = b = 3.2$ is about 10 GHz higher than a laser with a negative $b' = -1.5$ when both are stably locked under the same detuning frequency and injection strength. Thus a large, positive value of b' is favored for modulation bandwidth enhancement by stable injection locking. Although f_{pk} is a good indicator of the modulation bandwidth at a given operating point it does not reflect the actual bandwidth, especially in certain parts of the stable locking region. At high injection strengths, the modulation response dips by more than 3 dB in an intermediate frequency region between the zero frequency (i.e., DC) and f_{pk}. This dip could severely affect the modulation characteristics of the stably injection locked laser. One method to remove it is to use a cascaded optical injection configuration [124]. The first stage can be detuned to a more negative frequency to reach a high resonance frequency, and then the second stage is utilized to compensate the response reduction at the intermediate frequencies. Removal of the dip in the response spectrum without the need of a complex two-stage configuration can be accomplished by using a laser that has a small or negative b' factor, as illustrated in Fig. 4.3. For a semiconductor laser of $b = b' = 3.2$ the dip of the modulation response at the intermediate frequencies causes a significant reduction of its 3-dB modulation bandwidth; it is reduced from 38.2 GHz to 15.8 GHz when the laser is injection-locked at a detuning frequency of $f = -5$ GHz. Using a semiconductor laser that has the same $b = 3.2$ but a slightly smaller $b' = 1.5$ increases the 3-dB modulation bandwidth to 36.4 GHz by reducing the response dip at the intermediate frequencies. Further reduction in the gain saturation factor continues to raise the response at the intermediate frequencies but at a cost of reducing the modulation bandwidth due to a reduction in the relaxation resonance frequency.

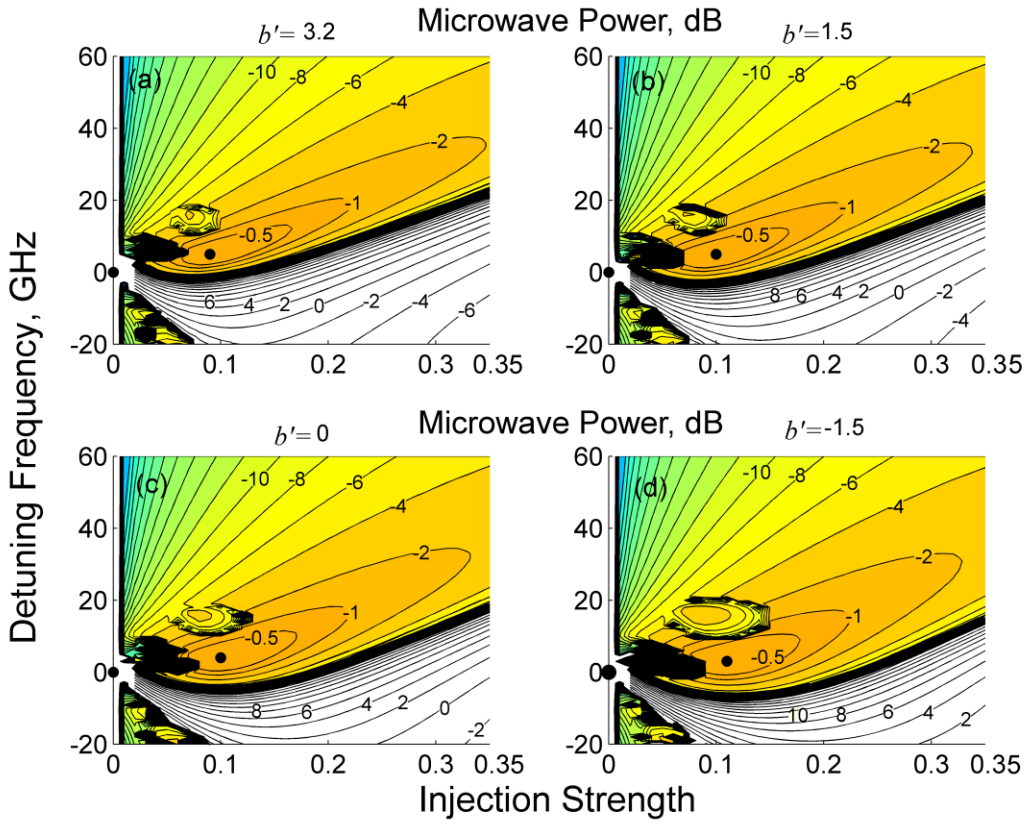

Figure 4.4: Power maps, as functions of the optical injection strength and detuning frequency, at $\tilde{J}$ = 1.222. The contour curves represent a constant power level for the P1 power (colored region), normalized in dB to its maximum indicated by a black dot, and P_{pk} (uncolored region), normalized in dB to its free-running power at ξ = 0 and f = 0, indicated by a black dot. The thick curve represents the Hopf bifurcation line. The second dense curve represents the period-doubling bifurcation. Black regions indicate chaos. The gain saturation factor is varied with (a) b' = b = 3.2, (b) b' = 1.5, (c) b' = 0 and (d) b' = −1.5 while the other laser parameters are held constant.

Figure 4.4 shows the mapping of the modulation resonance peak power, P_{pk}, normalized in dB to its free-running power at $\xi = 0$ and $f = 0$, indicated by a black dot. As in previous mappings, the thick black curve in Fig. 4.4 is the Hopf bifurcation line separating the stable locking region from periodic oscillations. Below the Hopf bifurcation line are contour curves representing constant values of P_{pk} at different operating conditions. As the operating point is shifted towards a more negative detuning frequency and a higher injection strength away from the Hopf bifurcation line, P_{pk} is reduced. As seen in Fig. 4.3, although f_{pk} of a stably injection-locked laser increases with the value of its b' factor when all other parameters of the laser are fixed, the response power P_{pk} at f_{pk} decreases due to the response dip. This effect is seen by comparing Fig. 4.4(a)–(d) where P_{pk} for a laser that is stably locked with a fixed detuning frequency and a fixed injection strength increases when the value of b' decreases from 3.2 to 1.5, 0, and −1.5.

Direct modulation generates two signal sidebands on the two sides of the optical carrier. In a radio-over-fiber transmission system, the double-sideband (DSB) spectrum leads to degradation in the RF signals associated with the phase walk-off between the two sidebands caused by fiber dispersion. The severe microwave power penalty due to DSB modulation can be significantly reduced by using SSB modulation [23]. Direct modulation of an optically injected semiconductor laser in stable locking generates nearly SSB modulation for a laser with $b \neq b'$ [125]. The SSB spectrum results from the suppression of the high frequency sideband with respect to the low-frequency sideband due to the antiguidance effect characterized by the b and b' factors. The degree of the asymmetry between the two sidebands is measured by the SRR, which is defined as the ratio, measured in dB, of the high-power low-frequency sideband to the low power high-frequency sideband. Figure 4.5 shows the SRR

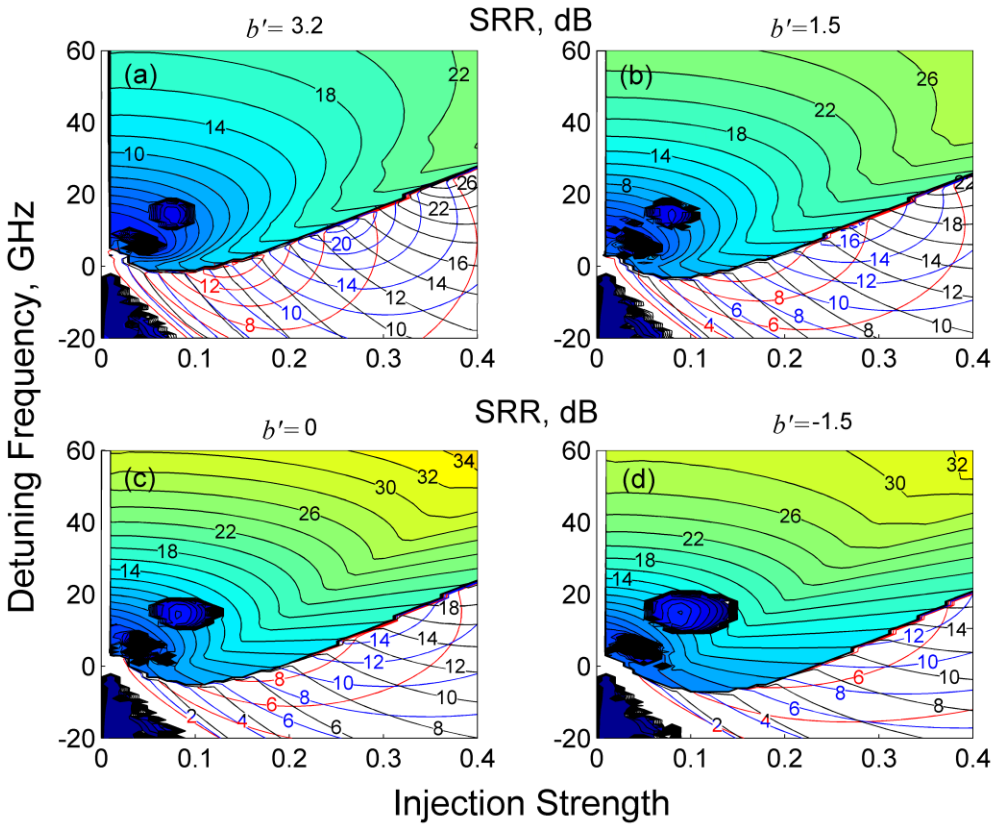

Figure 4.5: SRR maps, as functions of the optical injection strength and detuning frequency at $\tilde{J}$ = 1.222. The contour curves represent the SRR, in dB, of the P1 dynamic (colored region) and in the stably injection-locked laser (uncolored region), at different modulation frequencies: $f_{\tilde{J}}$ = 10 GHz (red), $f_{\tilde{J}}$ = 20 GHz (blue) and $f_{\tilde{J}}$ = 30 GHz (black). The thick curve represents the Hopf bifurcation line. The second dense curve represents the period-doubling bifurcation. Black regions indicate chaos. The gain saturation factor is varied with (a) b' = b = 3.2, (b) b' = 1.5, (c) b' = 0 and (d) b' = −1.5 while the other laser parameters are held constant.

for different injection strengths and detuning frequencies for four lasers of b' equal to 3.2, 1.5, 0 and −1.5 in Fig. 4.5(a)–(d), respectively. The contour curves below the Hopf bifurcation line represent a constant SRR for the stably injection-locked laser. The three sets of contour curves in different colors represent the SRR for different modulation frequencies at f_J = 10 GHz (red), f_J = 20 GHz (blue) and f_J = 30 GHz (black). For fixed b' and f_J, the highest SRR is reached at an operating point closest to the Hopf bifurcation line. Comparing the SRR at different f_J with its corresponding f_{pk} in Fig. 4.2 for the same laser at a fixed operating point, it is seen that the highest SRR is attained at a modulation frequency just below f_{pk}. Finally, a comparison between lasers of different b' at the same operating point and f_J finds the highest SRR of up 26 dB for a laser with $b' = b = 3.2$, as demonstrated in Fig. 4.5(a). As b' is reduced a decrease in the SSB modulation capabilities is seen at the same operating point, as illustrated in Fig. 4.5(b)–(d).

4.4 Effects on Period-One Dynamics

The P1 dynamics induced by optical injection can reach frequencies of more than 6 times the relaxation resonance frequency of the free-running laser [23]. Recently, such P1 dynamics have been studied for radio-over-fiber applications [23], [87], showing optically controlled tunability over a broad, continuous P1 frequency range for the uplink subcarrier frequency, which exceeds the laser modulation bandwidth. Figure 4.6 shows the characteristics of the P1 dynamics as functions of b' value when it is continuously varied from −3.2 to 3.2 at different operating points of the optically injected laser. Fig. 4.6(a) shows the optical spectrum of a typical P1 dynamic, where the main frequency components are shown with frequency offsets equal to the P1 frequency f_0. The primary oscillation spectral line, $f - f_0$, of

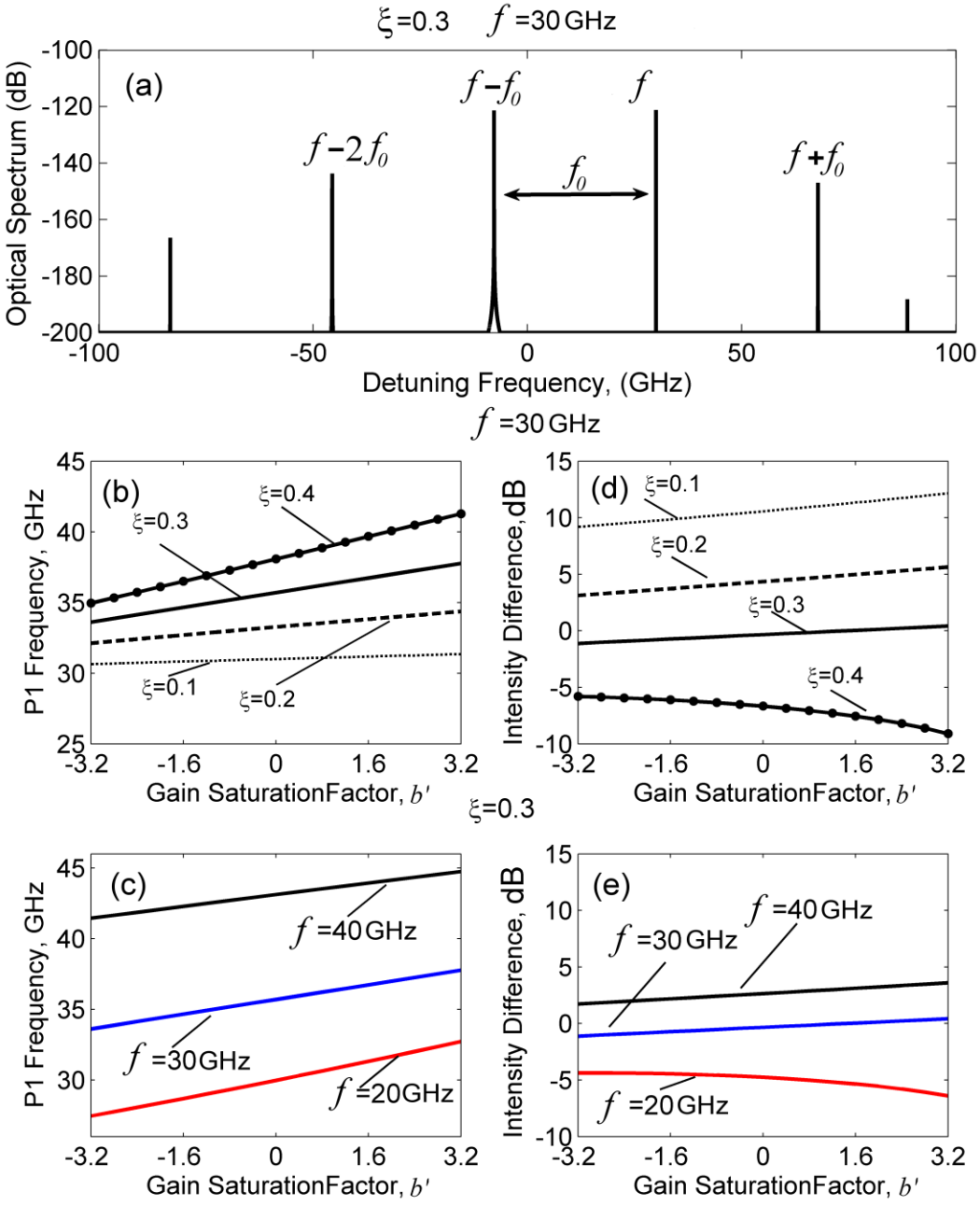

Figure 4.6: (a) A typical optical spectrum in the P1 dynamics at ξ = 0.3 and f = 30 GHz for b' = 3.2. (b)–(e) Frequency separation (P1 frequency)and intensity difference of the primary oscillation component relative to the injection frequency component in the optical spectrum as a function of b' under a fixed detuning frequency of f = 30 GHz (upper row) for four different injection levels and under a fixed injection strength of ξ = 0.3 (bottom row) for three different detuning frequencies.

the P1 dynamic in the optical spectrum is defined as the frequency component that is closest to the cavity resonance of the injected laser other than the injection frequency spectral line, f [50]. This primary oscillation component is generally the lower sideband of the injection-locked laser frequency due to the positive value of the linewidth enhancement factor b. Fig. 4.6(b) and (c) show the P1 frequency f_0 in the optical spectrum at a fixed detuning frequency of f = 30 GHz and at a fixed injection strength of ξ = 0.3, respectively. Fig. 4.6(d) and (e) show the intensity difference, in dB, of the intensity at $f - f_0$ spectral line relative to the intensity at the f line, which represents the asymmetry of the optical spectrum, at a fixed detuning frequency of f = 30 GHz and a fixed injection strength of ξ = 0.3, respectively. The intensity at the f spectral line and that at the $f - f_0$ spectral line are both larger than the intensity of the higher sideband, $f + f_0$, and the lower sideband, $f - 2\ f_0$, in the optical spectrum; therefore, the $f + f_0$ and $f - 2\ f_0$ spectral lines will not be addressed here. Similar to the effects of the linewidth enhancement factor, increasing the gain saturation factor shifts the $f - f_0$ line away from the f line, thus increasing the P1 frequency [118], as seen in Fig. 4.6(b). This effect is enhanced as the injection strength is increased. The higher the injection strength is, the faster the $f - f_0$ line shifts away from the f line as b' is increased. Similarly, Fig. 4.6(c) shows that at a fixed injection strength, the P1 frequency increases consistently for different detuning frequencies as b' is increased. The intensity difference in Fig. 4.6(d) shows that at low injection strengths the intensity at the $f - f_0$ line is higher than that at the f line. As the injection strength is increased, the intensity at the f line increases and eventually surpasses that at the $f - f_0$ line, resulting in a negative intensity difference. For ξ = 0.1, 0.2 and 0.3, a monotonic increase in the intensity difference is observed as b' is increased. However, for ξ = 0.4, increasing the value of b' causes a drop in the intensity difference. Figure

4.6(e) shows a monotonic increase in the intensity difference as b' is increased, for detuning frequencies of 30 GHz and 40 GHz. At a lower detuning frequency of f = 20 GHz, the intensity difference decreases as b' increases. These observations indicate that the addition of an external optical field reduces the carrier density, which results in the reduction of the necessary gain of the injected laser, and therefore an increase in the refractive index of the gain medium through b and b'. Consequently, the laser field experiences an increased cavity length and a reduction in the cavity resonance frequency, thus lowering the frequency of the $f - f_0$ line. Because the laser frequency is locked by the injection frequency, this effect leads to an increase in the P1 frequency, which is the separation between the $f - f_0$ and f spectral lines, as the value of b or b' is increased under fixed injection conditions, as observed in Fig. 4.6(b) and (c). Meanwhile, an increase in intensity difference is expected due to the increase in the intensity at the $f - f_0$ line, as observed in Fig. 4.6(d) and (e). This does not happen, however, at high injection strengths or at low detuning frequencies where the f spectral line is favored and a drop in the intensity difference is observed, as seen in Fig. 4.6(d) for the case of ξ = 0.4 and in Fig. 4.6(e) for the case of f = 20 GHz. The P1 frequency at high injection strengths is more sensitive to the change in b' than at low injection strengths, as seen in Fig. 4.6(b). However, the effects of the change in b' on the P1 frequency is most significant in the neighborhood of the chaotic regions, at low injection strengths and low detuning frequencies, where the system is highly nonlinear, as seen in Fig. 4.2. In this map area of low injection strengths and low detuning frequencies, the contour curves for the P1 frequency bend at sharper angles as b' is increased. This characteristic makes pinpointing the b' value essential for accurately fitting experimental data at low injection strengths and low detuning frequencies as demonstrated in Chapter 3. One of the key features that is sensitive to b' is the

lowest point of the Hopf bifurcation curve in the map [126, 127]. Other important features in this area that also depend on b' are the regions of advanced dynamics [44, 114] and the LS points. The sharp turning of the contour curves in this area is attributed to the competition between the red shifting of the cavity resonance frequency caused by the antiguidence effect and the Adler-type pulling effect. At high detuning frequencies, the red shifting of the cavity resonance frequency causes frequency pushing, whereas at low detuning frequencies close to the free-running laser frequency the Adler-type pulling dominates. This competition between these two phenomena originates from the existence of two limit cycles of different frequencies that coalesce in the area above the chaotic region in a saddle node bifurcation of limit cycles [40]. For completeness, Fig. 4.4 shows the power of the P1 oscillation in the colored region above the Hopf bifurcation line. The contour curves show the P1 power normalized to the maximum P1 power, which is shown as a black dot. Contrary to the strong dependence on b' of the modulation resonance peak power P_{pk} in the stable locking region, b' has no significant effect on the power of the P1 oscillation. In Fig. 4.4 the contour curves for all power levels in the P1 region above the Hopf bifurcation line only slightly change as the b' value is varied.

The SSB modulation capabilities of the laser under stable injection locking discussed in the preceding section show optimum performance for a laser with $b' = b$ at operational points close to the Hopf bifurcation line with a modulation frequency just below f_{pk}. An optically injected semiconductor laser operating in a P1 dynamic generally has better SSB modulation capabilities than operating in stable locking. The spectrum of a P1 dynamic consists of highly intensity-asymmetric sidebands that are equally separated from the injection-locked laser oscillation frequency. Recently P1 dynamics have been used for DSB to SSB

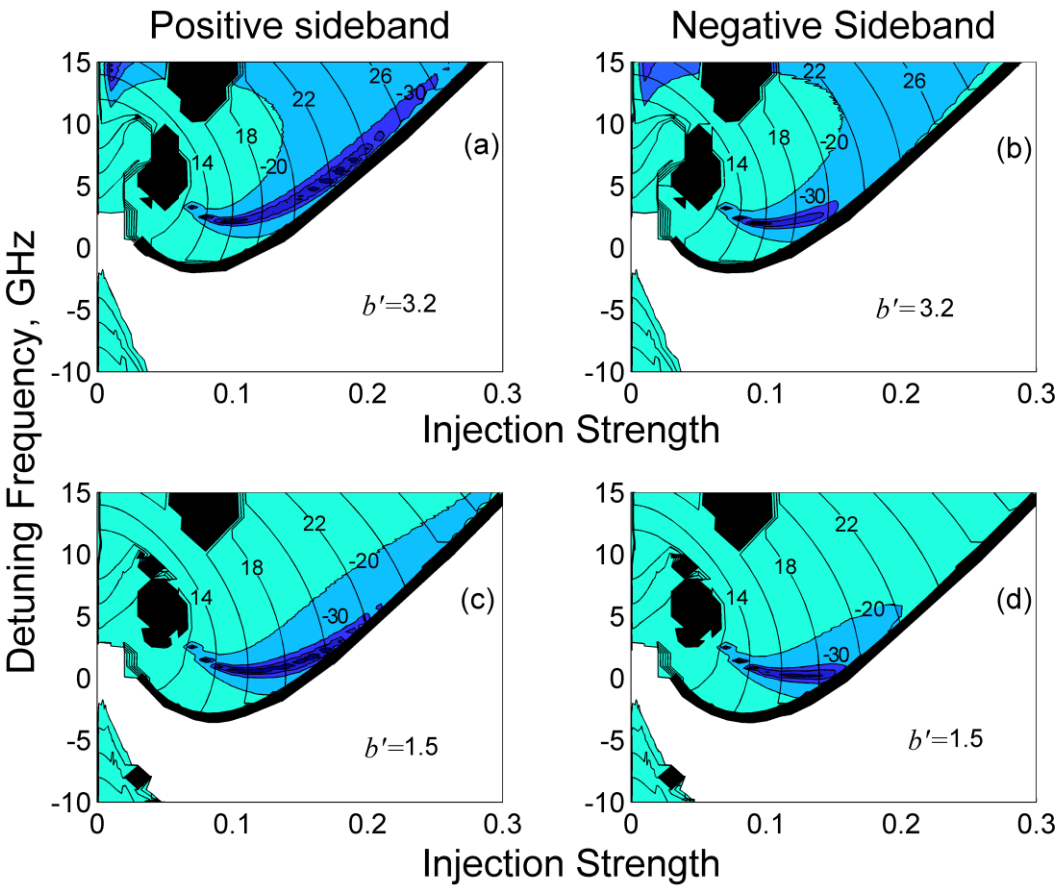

Figure 4.7: Mappings of the LS regions as functions of the optical injection strength and detuning frequency at $\tilde{J}$ = 1.222. The contour curves represent a constant P1 frequency, in GHz. The colored regions represent the amount of sideband suppression with respect to the carrier, in dBc, under a weak current modulation at $f_{\tilde{J}}$ = 100 MHz for the positive (left column) and negative (right column) sidebands. Stable locking (uncolored region) and complex dynamics (black regions) are shown across the Hopf bifurcation line (thick curve). The gain saturation factor is varied with (a)–(b) b' = b = 3.2, (c)–(d) b' = 1.5 while the other laser parameters are held constant

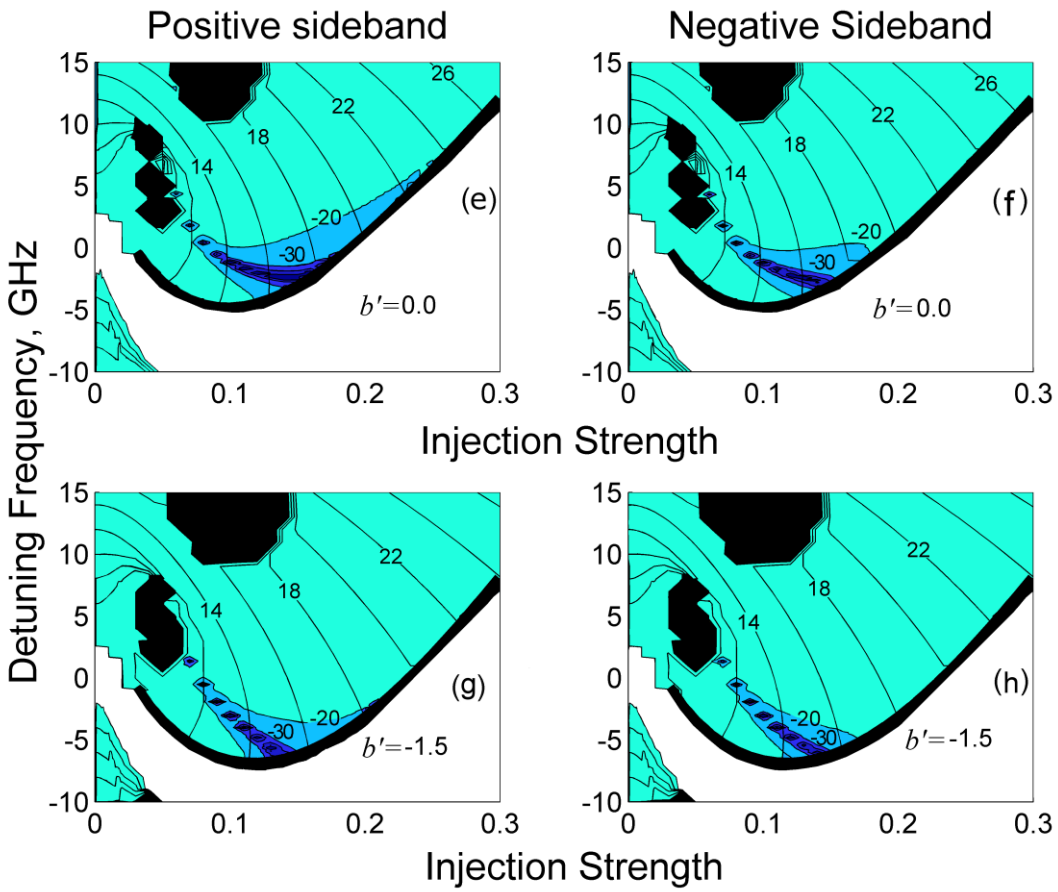

Continue Figure 4.7: Mappings of the LS regions as functions of the optical injection strength and detuning frequency at $\tilde{J}$ = 1.222. The contour curves represent a constant P1 frequency, in GHz. The colored regions represent the amount of sideband suppression with respect to the carrier, in dBc, under a weak current modulation at $f_{\tilde{J}}$ = 100 MHz for the positive (left column) and negative (right column) sidebands. Stable locking (uncolored region) and complex dynamics (black regions) are shown across the Hopf bifurcation line (thick curve). The gain saturation factor is varied with (e)–(f) b' = 0 and (g)–(h) b' = −1.5 while the other laser parameters are held constant.

conversion of a frequency-modulated semiconductor laser in a master-slave configuration, leading to an increased modulation depth and an improvement in microwave amplification and detection sensitivity [98]. The asymmetry of the optical spectrum of a P1 dynamic is measured by the SRR. The weaker of the two dominating components is first chosen. It is then compared with the strongest component among the rest of the sidebands. The power difference in dB is defined as SRR. Figure 4.5 shows the SRR of P1 dynamics in the colored region above the Hopf bifurcation line for four different values of gain saturation factor b' = 3.2, 1.5, 0 and −1.5 while other laser parameters are fixed. For $b' = b = 3.2$, the SRR can reach 22 dB at high injection strengths, as seen in Fig. 4.5(a). Reduction in the value of b' increases the SSB modulation capabilities of P1 dynamics until a maximum SRR is reached at $b' = 0$, as seen in Fig. 4.5(c). Further reduction in b' to a negative value reduces the SRR, as seen in Fig. 4.5(d). Therefore, a semiconductor laser operating close to the gain peak, where $b' \approx 0$, has the best SSB modulation capability relative to DSB modulation for a minimal microwave power fluctuation over the fiber transmission distance.

The significance of the b' factor on the P1 frequencies of low-sensitivity to fluctuations has been observed in the experimental data fitting done in Chapter 3. To demonstrate the dependency of the LS points on the b' factor mappings of the LS points are calculated for lasers of different b' factors. The results are shown in Fig. 4.7, which shows the LS_J operating conditions and their dependence on b', through mapping of the positive (left column) and negative (right column) modulation sidebands with respect to the carrier at the P1 frequency when a weak current modulation at f_J = 100 GHz is applied. The contour curves show the P1 frequencies, whereas the colors represent the amount of modulation sideband suppression as in mappings of Chapter 3. Black colored regions represent complex dynamics. For the case

of $b' = b = 3.2$, large regions colored in light blue for 20 dBc suppression of the sidebands are seen in Fig. 4.7(a) and (b). Around the $LS_{\tilde{J}}$ points at the local minima of P1 frequency contour curves, large suppression of the modulation sidebands as high as 50 dBc (dark blue) is observed, indicating highly stable P1 oscillations in this region. Reduction in the b' value significantly shrinks the stable P1 regions, but the large suppression of the modulation sidebands up to 50 dBc remains in the neighborhood of the $LS_{\tilde{J}}$ points. Similar effects of b' on the LS_{ξ} and LS_{f} is observed when modulation is added on the master laser amplitude or modulation on the master laser frequency, respectively, for different combination mappings of ξ - f, ξ - $\tilde{J}$, and $\tilde{J}$ - f. Therefore, for lasers of small or negative b' values, highly stabilized P1 oscillations still exist, though in smaller and more restricted regions. It is worth noting that as opposed to the gain saturation factor b', a large value of the linewidth enhancement factor b reduces the $LS_{\tilde{J}}$ regions around the $LS_{\tilde{J}}$ points.

Complex dynamics occupy small regions in the dynamics maps relative to P1 dynamics and stable locking. Nonetheless, complex dynamics possess significant attributes that make them useful in various applications. The P2 regions in the maps broaden significantly when the value of b' is reduced, as seen in Fig. 4.2 in the broadening of the area encircled by the second dense curve that indicates period-doubling bifurcation. Chaotic oscillations, on the other hand are relatively unaffected by the change in the b' value, as seen in the dark regions in Fig. 4.2 above the Hopf bifurcation line. A study on the chaotic oscillations induced by optical injection for lasers with different b' values did not show any significant influence on the bandwidth of chaos.

4.5 Summary

The significance of the gain saturation factor b' for an optically injected semiconductor laser emerges in the characteristics of the nonlinear phenomena induced by injection locking. Instability of the induced dynamics, measured by the expansion of regions of periodic oscillations through suppression of the stable locking region, is favored by a small or negative b' in contrast to the opposite effect of the linewidth enhancement factor b. Under similar operating conditions, an optically injection-locked semiconductor laser that has a larger or positive b' tends to reach higher relaxation resonance frequencies than ones that have a small or negative b'. This high relaxation resonance frequency is usually accompanied by a reduction, rather than an increase, in the modulation bandwidth due to a dip of the modulation response in the intermediate frequency region at high injection strengths. To an extent, this reduction in the 3-dB modulation bandwidth of the optically injection laser can be resolved by using a laser that has a small or negative b' factor to smooth out the modulation response curve across the spectrum. For similar operating conditions, a large positive b' leads to favorable SSB capabilities for a stably injection-locked laser, whereas the most favorable SSB capabilities for the P1 dynamics of an optically injected laser occur when the laser operates close to the gain peak when $b' \approx 0$. The P1 frequency at a low injection strength is highly sensitive to the variation in b'. A large or more positive b' produces more stable P1 oscillations in regions of the dynamics map around the LS points located at the local minima of P1 frequency contour curves. Higher dynamics such as P2 are also affected by the value of b', but the chaotic dynamics are found to be relatively unaffected. The value of b' considerably depends on the gain medium and the laser structure. For example, it can be varied by shifting the emission wavelength of a DFB laser from its gain peak. Therefore, desirable dynamical charac-

teristics found in this study can be reached by properly tuning the laser to a desirable value of b'.

CHAPTER 5

Conclusion

The work presented in this dissertation shows the ability to control the limit-cycle dynamics of an optically injected semiconductor laser for the generation of narrow linewidth photonic microwaves. Theoretical simulations and experimental demonstration showed that the nonlinear dynamics of the laser could be controlled through the operational parameters of the optical injection system or through the intrinsic parameters of the laser. Various types of P1 oscillations with reduced sensitivity to fluctuations in the operational parameters and intrinsic laser noise have been discovered. P1 oscillations induced by optical injection at LS_{ξ}, LS_{f}, and LS_{J} points show reduced sensitivity to the effects of bias current and temperature fluctuations of the two lasers on the injection strength, detuning frequency and slave laser bias current, respectively. P1 oscillations with reduced sensitivity to two or more operational parameters exist at points where two or more P1 frequency extrema overlap. The gain saturation factor of the semiconductor laser plays a crucial role in the nonlinear dynamics induced by optical injection. The value of the b' factor depends on whether the laser operates on the red or the blue side of the gain peak. Controlling the value the b' can alter the characteristics of the nonlinear dynamics. It is shown that in both stable locking and periodic dynamics, a laser of a positive gain saturation factor that is smaller than the linewdith enhancement factor is most suitable for optical transmission requirements.

The results demonstrated in this dissertation are interesting on two levels: from a fundamental standpoint, the agreement between theory and model allows for new avenues of the tests of semiconductor laser characteristics and the measurements of the intrinsic parameters

based on the interactions described here. For example, there is considerable current interest in the dynamics of quantum-dot lasers and the precision of the techniques described here will allow rigorous testing of proposed modifications to the coupled equation model to characterize these novel structures [128, 129]. The second interesting aspect of this work is that photonic oscillators have been proposed for a variety of applications and the discovery of these low-sensitivity operating points shows that the optically injected laser may be able to display favorable characteristics of reduced phase noise and jitter to go along with its wide tuning range and SSB capabilities. Now additional work is needed to see if these observations can be translated into improved performance of photonic devices such as broadly tunable, low-noise, low-jitter oscillators.

In the future, more research efforts shall be devoted to low-sensitivity points in nonlinear oscillators. Theoretical analysis on nonlinear oscillators that invoke limit-cycle dynamics can be studied to develop analytical models that carry the systems nonlinearities. Theories that rely on perturbation analysis to solve for the limit-cycle dynamics often become inaccurate for quantitatively describing the optical injection system in the P1 region [130]. A newly developed method uses the two dominant optical frequency components to approximate the P1 frequency at regions where the P1 frequency is larger than the relaxation resonance frequency of the laser [116]. This approach cannot yield quantitative results when the system is highly nonlinear in regions where the P1 frequency is smaller than the relaxation resonance frequency of the laser. A linearized analysis of the optical injection system, although capable of quantitatively solving the system in the stable locking region, cannot quantitatively yield the P1 frequency in the high nonlinear regions either [42]. A recent method that can get excellent quantitative results uses the general limit-cycle solution and takes into account

high-order harmonics [117]. Expanding on this technique, we can further study the low-sensitivity points in the optical injection system to further explore the oscillator nonlinearities for reducing the effects of noise and improving the frequency precision of other nonlinear oscillators that invoke limit-cycle dynamics.

REFERENCES

[1] J. Capmany and D. Novak, " Microwave photonics combines two worlds," *Nat. Photonics,* vol. 1, p. 319, 2007.

[2] A. J. Seeds and K. J. Williams, "Microwave Photonics," *J. Lightwave Technol.,* vol. 24, pp. 4628-4641, 2006.

[3] J. Yao, "Microwave Photonics," *J. Lightwave Technol.,* vol. 27, pp. 314-335, 2009.

[4] R. A. Minasian, "Photonic signal processing of microwave signals," *IEEE Trans. Microwave Theory Tech.,* vol. 54, pp. 832-846, 2006.

[5] X. Q. Qi and J. M. Liu, "Photonic Microwave Applications of the Dynamics of Semiconductor Lasers," *IEEE J. Sel. Top. Quantum Electron.,* vol. 17, pp. 1198-1211, 2011.

[6] R. Tucker, "High-speed modulation of semiconductor lasers," *Electron Devices, IEEE Transactions on,* vol. 32, pp. 2572-2584, 1985.

[7] J. M. Liu, *Photonic Devices*. Cambridge University Press, 2005.

[8] O. Kjebon, R. Schatz, S. Lourdudoss, S. Nilsson, B. Stalnacke, and L. Backbom, "30 GHz direct modulation bandwidth in detuned loaded InGaAsP DBR lasers at 1.55um wavelength," *Electron. Lett.,* vol. 33, pp. 488-489, 1997.

[9] J. J. O'Reilly, P. M. Lane, R. Heidemann, and R. Hofstetter, "Optical generation of very narrow linewidth millimetre wave signals," *Electron. Lett.,* vol. 28, pp. 2309-2311, 1992.

[10] T. Ido, S. Tanaka, M. Suzuki, M. Koizumi, H. Sano, and H. Inoue, "Ultra-high-speed multiple-quantum-well electro-absorption optical modulators with integrated waveguides," *J. Lightwave Technol.,* vol. 14, pp. 2026-2034, 1996.

[11] A. Karim and J. Devenport, "Noise Figure Reduction in Externally Modulated Analog Fiber-Optic Links," *IEEE Photon. Technol. lett.,* vol. 19, pp. 312-314, 2007.

[12] U. Gliese, T. N. Nielsen, S. Norskov, and K. E. Stubkjaer, "Multifunctional fiber-optic microwave links based on remote heterodyne detection," *IEEE Trans. Microwave Theory Tech.,* vol. 46, pp. 458-468, 1998.

[13] R. T. Ramos and A. J. Seeds, "Fast heterodyne optical phase-lock loop using double quantum well laser diodes," *Electron. Lett.,* vol. 28, pp. 82-83, 1992.

[14] U. Gliese, T. N. Nielsen, M. Bruun, E. Lintz Christensen, K. E. Stubkjaer, S. Lindgren, and B. Broberg, "A wideband heterodyne optical phase-locked loop for generation of 3-18 GHz microwave carriers," *IEEE Photon. Technol. lett.*, vol. 4, pp. 936-938, 1992.

[15] S. K. Hwang, J. M. Liu, and J. K. White, "35-GHz Intrinsic Bandwidth for Direct Modulation in 1.3-um Semiconductor Lasers Subject to Strong Injection Locking," *IEEE Photonics Technol. Lett.*, vol. 16, pp. 972-974, 2004.

[16] L. Goldberg, H. F. Taylor, J. F. Weller, and D. M. Bloom, "Microwave signal generation with injection-locked laser diodes," *Electron. Lett.*, vol. 19, pp. 491-493, 1983.

[17] A. C. Bordonalli, B. Cai, A. J. Seeds, and P. J. Williams, "Generation of microwave signals by active mode locking in a gain bandwidth restricted laser structure," *IEEE Photon. Technol. lett.*, vol. 8, pp. 151-153, 1996.

[18] D. J. Derickson, R. J. Helkey, A. Mar, J. G. Wasserbauer, Y. G. Wey, and J. E. Bowers, "Microwave and millimeter wave signal generation using mode-locked semiconductor lasers with intra-waveguide saturable absorbers," *IEEE MTT-S Int. Microw. Symp. Dig*, pp. 753-756 vol.2, 1992.

[19] X. S. Yao and L. Maleki, "Optoelectronic oscillator for photonic systems," *IEEE J. Quantum Electron.*, vol. 32, pp. 1141-1149, 1996.

[20] D. Wake, C. R. Lima, and P. A. Davies, "Optical generation of millimeter-wave signals for fiber-radio systems using a dual-mode DFB semiconductor laser," *IEEE Trans. Microwave Theory Tech.*, vol. 43, pp. 2270-2276, 1995.

[21] L. A. Johansson, Z. Hu, D. J. Blumenthal, L. A. Coldren, Y. A. Akulova, and G. A. Fish, "40-GHz dual-mode-locked widely tunable sampled-grating DBR laser," *IEEE Photon. Technol. lett.*, vol. 17, pp. 285-287, 2005.

[22] S. Strogatz, *Nonlinear dynamics and chaos with applications to physics, biology, chemistry, and engineering*. Westview Press, 2000.

[23] S. C. Chan, S. K. Hwang, and J. M. Liu, "Period-one oscillation for photonic microwave transmission using an optically injected semiconductor laser," *Opt. Express*, vol. 15, pp. 14921-14935, 2007.

[24] S. K. Hwang, J. M. Liu, and J. K. White, "Characteristics of period-one oscillations in semiconductor lasers subject to optical injection," *IEEE J. Sel. Top. Quantum Electron.*, vol. 10, pp. 974-981, 2004.

[25] H. Haken, "Analogy between higher instabilities in fluids and lasers," *Physics Letters A*, vol. 53, pp. 77-78, 1975.

[26] E. N. Lorenz, "Deterministic Nonperiodic Flow," *J. Atmos. Sci.*, vol. 20, pp. 130-141, 1963.

[27] F. T. Arecchi, G. L. Lippi, G. P. Puccioni, and J. R. Tredicce, "Deterministic chaos in laser with injected signal," *Opt. Commun.*, vol. 51, pp. 308-314, 1984.

[28] N. B. Abraham, L. A. Lugiato, and L. M. Narducci, "Overview of instabilities in laser systems," *J. Opt. Soc. Am. B*, vol. 2, pp. 7-14, 1985.

[29] G. P. Agrawal, *Fiber-optic communication system*. Wiley-Interscience, 2002.

[30] A. E. Siegman, *Lasers*. University Science Books, 1986.

[31] G. H. M. V. Tartwijk and D. Lenstra, "Semiconductor lasers with optical injection and feedback," *J. Opt. B: Quantum Semiclassical Opt.*, vol. 7, p. 87, 1995.

[32] J. Sacher, D. Baums, P. Panknin, W. Elsässer, and E. O. Göbel, "Intensity instabilities of semiconductor lasers under current modulation, external light injection, and delayed feedback," *Phys. Rev. A*, vol. 45, pp. 1893-1905, 1992.

[33] Y. C. Chen, H. G. Winful, and J. M. Liu, "Subharmonic bifurcations and irregular pulsing behavior of modulated semiconductor lasers," *Appl. Phys. Lett.*, vol. 47, pp. 208-210, 1985.

[34] E. Hemery, L. Chusseau, and J. M. Lourtioz, "Dynamic behaviors of semiconductor lasers under strong sinusoidal current modulation: modeling and experiments at 1.3um," *IEEE J. Quantum Electron.*, vol. 26, pp. 633-641, 1990.

[35] C. H. Lee, T. H. Yoon, and S. Y. Shin, "Period doubling and chaos in a directly modulated laser diode," *Appl. Phys. Lett.*, vol. 46, pp. 95-97, 1985.

[36] G. Carpintero and H. Lamela, "Intermittent bursts in a directly modulated laser diode," *IEEE J. Quantum Electron.*, vol. 36, pp. 1284-1292, 2000.

[37] H. F. Liu and W. F. Ngai, "Nonlinear dynamics of a directly modulated 1.55um InGaAsP distributed feedback semiconductor laser," *IEEE J. Quantum Electron.*, vol. 29, pp. 1668-1675, 1993.

[38] R. Lang, "Injection locking properties of a semiconductor laser," *IEEE J. Quantum Electron.*, vol. 18, pp. 976-983, 1982.

[39] I. Petitbon, P. Gallion, G. Debarge, and C. Chabran, "Locking bandwidth and relaxation oscillations of an injection-locked semiconductor laser," *IEEE J. Quantum Electron.,* vol. 24, pp. 148-154, 1988.

[40] S. Wieczorek, B. Krauskopf, T. B. Simpson, and D. Lenstra, "The dynamical complexity of optically injected semiconductor lasers," *Phys. Rep.,* vol. 416, pp. 1-128, 2005.

[41] T. B. Simpson, J. M. Liu, K. F. Huang, K. Tai, C. M. Clayton, A. Gavrielides, and V. Kovanis, "Cavity enhancement of resonant frequencies in semiconductor lasers subject to optical injection," *Phys. Rev. A,* vol. 52, pp. R4348-R4351, 1995.

[42] T. B. Simpson, J. M. Liu, and A. Gavrielides, "Small-signal analysis of modulation characteristics in a semiconductor laser subject to strong optical injection," *IEEE J. Quantum Electron.,* vol. 32, pp. 1456-1468, 1996.

[43] A. Murakami, K. Kawashima, and K. Atsuki, "Cavity resonance shift and bandwidth enhancement in semiconductor lasers with strong light injection," *IEEE J. Quantum Electron.,* vol. 39, pp. 1196-1204, 2003.

[44] T. B. Simpson, "Mapping the nonlinear dynamics of a distributed feedback semiconductor laser subject to external optical injection," *Opt. Commun.,* vol. 215, pp. 135-151, 2003.

[45] A. Gavrielides, T. Erneux, V. Kovanis, P. M. Alsing, and T. B. Simpson, "Subharmonic Resonances in an optically injected semiconductor laser: theory and experiments," *J. Opt. B: Quantum Semiclassical Opt.,* vol. 9, p. 575, 1997.

[46] J. Troger, L. Thevenaz, P. A. Nicati, and P. A. Robert, "Theory and Experiment of a Single-Mode Diode Laser Subject to External Light Injection from Several Lasers," *J. Lightwave Technol.,* vol. 17, p. 629, 1999.

[47] N. M. Al-Hosiny, I. D. Henning, and M. J. Adams, "Tailoring enhanced chaos in optically injected semiconductor lasers," *Opt. Commun.,* vol. 269, pp. 166-173, 2007.

[48] W. Li, N. H. Zhu, L. X. Wang, J. H. Ke, S. F. Chen, X. Q. Qi, B. H. Zhang, and L. Xie, "Frequency-Pushing Effect in Single-Mode Diode Laser Subject to External Dual-Beam Injection," *IEEE J. Quantum Electron.,* vol. 46, pp. 796-803, 2010.

[49] X. Q. Qi and J. M. Liu, "Dynamics Scenarios of Dual-Beam Optically Injected Semiconductor Lasers," *IEEE J. Quantum Electron.,* vol. 47, pp. 762-769, 2011.

[50] M. AlMulla, X. Q. Qi, and J. M. Liu, "Dynamics Maps and Scenario Transitions for a Semiconductor Laser Subject to Dual-Beam Optical Injection," *IEEE J. Sel. Top. Quantum Electron.,* vol. 19, p. 1501108, 2013.

[51] A. Consoli, A. Quirce, A. Valle, I. Esquivias, L. Pesquera, and J. M. García Tijero, "High-frequency signal generation using 1550 nm VCSEL subject to two-frequency optical injection," *SPIE,* vol. 8639, p. 8, 2013.

[52] P. Perez, A. Quirce, A. Valle, A. Consoli, I. Noriega, L. Pesquera, and I. Esquivias, "Photonic generation of microwave signals using a single-mode VCSEL subject to dual-beam orthogonal optical injection," *Photonics Journal, IEEE,* vol. PP, pp. 1-1, 2015.

[53] C. H. Lee, S. Y. Shin, and S. Y. Lee, "Optical short-pulse generation using diode lasers with negative optoelectronic feedback," *Opt. Lett.,* vol. 13, pp. 464-466, 1988.

[54] G. Giacomelli, M. Calzavara, and F. T. Arecchi, "Instabilities in a semiconductor laser with delayed optoelectronic feedback," *Opt. Commun.,* vol. 74, pp. 97-101, 1989.

[55] G. F. Li, R. K. Boncek, X. Wang, and D. H. Sackett, "Transient and optoelectronic feedback-sustained pulsation of laser diodes at 1300 nm," *IEEE Photon. Technol. lett.,* vol. 7, pp. 854-856, 1995.

[56] F. Y. Lin and J. M. Liu, "Nonlinear dynamics of a semiconductor laser with delayed negative optoelectronic feedback," *IEEE J. Quantum Electron.,* vol. 39, pp. 562-568, 2003.

[57] G. Q. Xia, S. C. Chan, and J. M. Liu, "Multistability in a semiconductor laser with optoelectronic feedback," *Opt. Express,* vol. 15, pp. 572-576, 2007.

[58] S. Tang and J. M. Liu, "Chaotic pulsing and quasi-periodic route to chaos in a semiconductor laser with delayed opto-electronic feedback," *IEEE J. Quantum Electron.,* vol. 37, pp. 329-336, 2001.

[59] R. Lang and K. Kobayashi, "External optical feedback effects on semiconductor injection laser properties," *IEEE J. Quantum Electron.,* vol. 16, pp. 347-355, 1980.

[60] K. Otsuka and J. L. Chern, "High-speed picosecond pulse generation in semiconductor lasers withincoherent optical feedback," *Opt. Lett.,* vol. 16, pp. 1759-1761, 1991.

[61] J. Mork, B. Tromborg, and J. Mark, "Chaos in semiconductor lasers with optical feedback: theory and experiment," *IEEE J. Quantum Electron.,* vol. 28, pp. 93-108, 1992.

[62] A. Ritter and H. Haug, "Theory of laser diodes with weak optical feedback. II. Limit-cycle behavior, quasi-periodicity, frequency locking, and route to chaos," *J. Opt. Soc. Am. B,* vol. 10, pp. 145-154, 1993.

[63] G. H. M. Van Tartwijk and M. San Miguel, "Optical feedback on self-pulsating semiconductor lasers," *IEEE J. Quantum Electron.,* vol. 32, pp. 1191-1202, 1996.

[64] J. P. Toomey, D. M. Kane, M. W. Lee, and K. A. Shore, "Nonlinear dynamics of semiconductor lasers with feedback and modulation," *Opt. Express,* vol. 18, pp. 16955-16972, 2010.

[65] F. Y. Lin and J. M. Liu, "Nonlinear dynamical characteristics of an optically injected semiconductor laser subject to optoelectronic feedback," *Opt. Commun.,* vol. 221, pp. 173-180, 2003.

[66] Y. H. Liao and F. Y. Lin, "Dynamical characteristics and their applications of semiconductor lasers subject to both optical injection and optical feedback," *Opt. Express*, vol. 21, pp. 23568-23578, 2013.

[67] R. M. Nguimdo, M. Khoder, J. Danckaert, G. Van der Sande, and G. Verschaffelt, "Fast phase response and chaos bandwidth enhancement in semiconductor lasers subject to optical feedback and injection," *Opt. Lett.,* vol. 39, pp. 5945-5948, 2014.

[68] M. Ueno and R. Lang, "Conditions for self-sustained pulsation and bistability in semiconductor lasers," *J. Appl. Phys.,* vol. 58, pp. 1689-1692, 1985.

[69] J. L. A. Dubbeldam and B. Krauskopf, "Self-pulsations of lasers with saturable absorber: dynamics and bifurcations," *Opt. Commun.,* vol. 159, pp. 325-338, 1999.

[70] S. Barbay, R. Kuszelewicz, and A. M. Yacomotti, "Excitability in a semiconductor laser with saturable absorber," *Opt. Lett.,* vol. 36, pp. 4476-4478, 2011.

[71] A. Hohl, A. Gavrielides, T. Erneux, and V. Kovanis, "Localized Synchronization in Two Coupled Nonidentical Semiconductor Lasers," *Phys. Rev. Lett.,* vol. 78, pp. 4745-4748, 1997.

[72] G. Kozyreff, A. G. Vladimirov, and P. Mandel, "Global Coupling with Time Delay in an Array of Semiconductor Lasers," *Phys. Rev. Lett.,* vol. 85, pp. 3809-3812, 2000.

[73] S. Tang, R. Vicente, M. C. Chiang, C. R. Mirasso, and J. M. Liu, "Nonlinear dynamics of semiconductor lasers with mutual optoelectronic coupling," *IEEE J. Sel. Top. Quantum Electron.,* vol. 10, pp. 936-943, 2004.

[74] H. Erzgräber, D. Lenstra, B. Krauskopf, E. Wille, M. Peil, I. Fischer, and W. Elsäßer, "Mutually delay-coupled semiconductor lasers: Mode bifurcation scenarios," *Opt. Commun.,* vol. 255, pp. 286-296, 2005.

[75] R. Vicente, S. Tang, J. Mulet, C. R. Mirasso, and J. M. Liu, "Synchronization properties of two self-oscillating semiconductor lasers subject to delayed optoelectronic mutual coupling," *Physical Review E,* vol. 73, p. 047201, 2006.

[76] S. Donati and S.-K. Hwang, "Chaos and high-level dynamics in coupled lasers and their applications," *Prog. Quantum Electron.,* vol. 36, pp. 293-341, 2012.

[77] F. Mogensen, H. Olesen, and G. Jacobsen, "Locking conditions and stability properties for a semiconductor laser with external light injection," *IEEE J. Quantum Electron.,* vol. 21, pp. 784-793, 1985.

[78] T. B. Simpson, J. M. Liu, K. F. Huang, and K. Tai, "Nonlinear dynamics induced by external optical injection in semiconductor lasers," *J. Opt. B: Quantum Semiclassical Opt.,* vol. 9, p. 765, 1997.

[79] A. Gavrielides, V. Kovanis, M. Nizette, T. Erneux, and T. B. Simpson, "Period three limit-cycles in injected semiconductor lasers," *J. Opt. B: Quantum Semiclassical Opt.,* vol. 4, p. 20, 2002.

[80] V. Kovanis, A. Gavrielides, T. B. Simpson, and J. M. Liu, "Instabilities and chaos in optically injected semiconductor lasers," *Appl. Phys. Lett.,* vol. 67, pp. 2780-2782, 1995.

[81] T. B. Simpson, J. M. Liu, A. Gavrielides, V. Kovanis, and P. M. Alsing, "Period-doubling cascades and chaos in a semiconductor laser with optical injection," *Phys. Rev. A,* vol. 51, pp. 4181-4185, 1995.

[82] F. Y. Lin and J. M. Liu, "Diverse waveform generation using semiconductor lasers for radar and microwave applications," *IEEE J. Quantum Electron.,* vol. 40, pp. 682-689, 2004.

[83] T. B. Simpson, J. M. Liu, M. AlMulla, N. G. Usechak, and V. Kovanis, "Limit-Cycle Dynamics with Reduced Sensitivity to Perturbations," *Phys. Rev. Lett.,* vol. 112, p. 23901, 2014.

[84] T. B. Simpson, J. M. Liu, M. AlMulla, N. G. Usechak, and V. Kovanis, "Tunable Oscillations in Optically Injected Semiconductor Lasers With Reduced Sensitivity to Perturbations," *J. Lightwave Technol.,* vol. 32, pp. 3749-3758, 2014.

[85] M. AlMulla and J. M. Liu, "Frequency-stabilized limit-cycle dynamics of an optically injected semiconductor laser," *Appl. Phys. Lett.,* vol. 105, p. 011122 2014.

[86] T. B. Simpson and F. Doft, "Double-locked laser diode for microwave photonics applications," *IEEE Photon. Technol. lett.,* vol. 11, pp. 1476-1478, 1999.

[87] C. Cuicui and S. C. Chan, "Performance Analysis on Using Period-One Oscillation of Optically Injected Semiconductor Lasers for Radio-Over-Fiber Uplinks," *IEEE J. Quantum Electron.,* vol. 48, pp. 490-499, 2012.

[88] L. Fan, Z. M. Wu, T. Deng, J.-G. Wu, X. Tang, J. J. Chen, M. Song, and G. Q. Xia, "Subharmonic Microwave Modulation Stabilization of Tunable Photonic Microwave Generated by Period-One Nonlinear Dynamics of an Optically Injected Semiconductor Laser," *J. Lightwave Technol.,* vol. 32, pp. 4058-4064, 2014.

[89] Y. H. Hung and S. K. Hwang, "Photonic microwave stabilization for period-one nonlinear dynamics of semiconductor lasers using optical modulation sideband injection locking," *Opt. Express,* vol. 23, pp. 6520-6532, 2015.

[90] T. B. Simpson, "Phase-locked microwave-frequency modulations in optically-injected laser diodes," *Opt. Commun.,* vol. 170, pp. 93-98, 1999.

[91] S. C. Chan and J. M. Liu, "Tunable narrow-linewidth photonic microwave generation using semiconductor laser dynamics," *IEEE J. Sel. Top. Quantum Electron.,* vol. 10, pp. 1025-1032, 2004.

[92] T. B. Simpson, J. M. Liu, M. AlMulla, N. Usechak, and V. Kovanis, "Linewidth Sharpening via Polarization-Rotated Feedback in Optically-Injected Semiconductor Laser Oscillators," *IEEE J. Sel. Top. Quantum Electron.,* vol. 19, p. 1500807, 2013.

[93] J. P. Zhuang and S. C. Chan, "Tunable photonic microwave generation using optically injected semiconductor laser dynamics with optical feedback stabilization," *Opt. Lett.,* vol. 38, pp. 344-346, 2013.

[94] J. P. Zhuang and S. C. Chan, "Phase noise characteristics of microwave signals generated by semiconductor laser dynamics," *Opt. Express,* vol. 23, pp. 2777-2797, 2015.

[95] K. H. Lo, S. K. Hwang, and S. Donati, "Optical feedback stabilization of photonic microwave generation using period-one nonlinear dynamics of semiconductor lasers," *Opt. Express,* vol. 22, pp. 18648-18661, 2014.

[96] Y. S. Juan and F. Y. Lin, "Photonic Generation of Broadly Tunable Microwave Signals Utilizing a Dual-Beam Optically Injected Semiconductor Laser," *Photonics Journal, IEEE,* vol. 3, pp. 644-650, 2011.

[97] P. Perez, A. Quirce, A. Consoli, A. Valle, I. Noriega, L. Pesquera, and I. Esquivias, "Dynamics of long-wavelength VCSELs subject to dual-beam optical injection," vol. 9134, pp. 913409-913409-11, 2014.

[98] Y. H. Hung, C. H. Chu, and S. K. Hwang, "Optical double-sideband modulation to single-sideband modulation conversion using period-one nonlinear dynamics of

semiconductor lasers for radio-over-fiber links," *Opt. Lett.*, vol. 38, pp. 1482-1484, 2013.

[99] Y. H. Hung and S. K. Hwang, "Photonic microwave amplification for radio-over-fiber links using period-one nonlinear dynamics of semiconductor lasers," *Opt. Lett.*, vol. 38, pp. 3355-3358, 2013.

[100] S. K. Hwang, H. F. Chen, and C. Y. Lin, "All-optical frequency conversion using nonlinear dynamics of semiconductor lasers," *Opt. Lett.*, vol. 34, pp. 812-814, 2009.

[101] S. C. Chan and J. M. Liu, "Microwave Frequency Division and Multiplication Using an Optically Injected Semiconductor Laser," *IEEE J. Quantum Electron.*, vol. 41, pp. 1142-1147, 2005.

[102] S. C. Chan, S. K. Hwang, and J. M. Liu, "Radio-over-fiber AM-to-FM upconversion using an optically injected semiconductor laser," *Opt. Lett.*, vol. 31, pp. 2254-2256, 2006.

[103] C. H. Chu, S. L. Lin, S. C. Chan, and S. K. Hwang, "All-Optical Modulation Format Conversion Using Nonlinear Dynamics of Semiconductor Lasers," *IEEE J. Quantum Electron.*, vol. 48, pp. 1389-1396, 2012.

[104] J. Xiong, R. Wang, T. Pu, T. Fang, J. Zheng, D. Chen, L. Huang, and X. F. Chen, "A Novel Approach to Realizing a Widely Tunable Single Passband Microwave Photonic Filter Based on Optical Injection," *IEEE J. Sel. Top. Quantum Electron.*, vol. 21, pp. 1-6, 2015.

[105] T. B. Simpson and J. M. Liu, "Phase and amplitude characteristics of nearly degenerate four-wave mixing in Fabry-Perot semiconductor lasers," *J. Appl. Phys.*, vol. 73, pp. 2587-2589, 1993.

[106] M. P. van Exter, W. A. Hamel, J. P. Woerdman, and B. R. P. Zeijlmans, "Spectral signature of relaxation oscillations in semiconductor lasers," *IEEE J. Quantum Electron.*, vol. 28, pp. 1470-1478, 1992.

[107] J. M. Liu and T. B. Simpson, "Four-wave mixing and optical modulation in a semiconductor laser," *IEEE J. Quantum Electron.*, vol. 30, pp. 957-965, 1994.

[108] D. Antonio, D. H. Zanette, and D. Lopez, "Frequency stabilization in nonlinear micromechanical oscillators," *Nat. Commun.*, vol. 3, 2012.

[109] L. G. Villanueva, E. Kenig, R. B. Karabalin, M. H. Matheny, R. Lifshitz, M. C. Cross, and M. L. Roukes, "Surpassing Fundamental Limits of Oscillators Using Nonlinear Resonators," *Phys. Rev. Lett.*, vol. 110, 2013.

[110] B. Yurke, D. S. Greywall, A. N. Pargellis, and P. A. Busch, "Theory of amplifier-noise evasion in an oscillator employing a nonlinear resonator," *Phys. Rev. A,* vol. 51, pp. 4211-4229, 1995.

[111] M. C. Cross, E. Kenig, and J.-M. Allen, "Building better oscillators using nonlinear dynamics and pattern formation," *Pramana - J Phys,* pp. 1-17, 2015.

[112] T. B. Simpson and J. M. Liu, "Spontaneous emission, nonlinear optical coupling, and noise in laser diodes," *Opt. Commun.,* vol. 112, pp. 43-47, 1994.

[113] J. B. Gao, S. K. Hwang, and J. M. Liu, "Effects of intrinsic spontaneous-emission noise on the nonlinear dynamics of an optically injected semiconductor laser," *Phys. Rev. A,* vol. 59, pp. 1582-1585, 1999.

[114] T. Fordell and Å. M. Lindberg, "Numerical stability maps of an optically injected semiconductor laser," *Opt. Commun.,* vol. 242, pp. 613-622, 2004.

[115] S. K. Hwang and J. M. Liu, "Dynamical characteristics of an optically injected semiconductor laser," *Opt. Commun.,* vol. 183, p. 11, 2000.

[116] S. C. Chan, "Analysis of an Optically Injected Semiconductor Laser for Microwave Generation," *IEEE J. Quantum Electron.,* vol. 46, pp. 421-428, 2010.

[117] C. J. Lin, M. AlMulla, and J. M. Liu, "Harmonic Analysis of Limit-Cycle Oscillations of an Optically Injected Semiconductor Laser," *IEEE J. Quantum Electron.,* vol. 50, pp. 815-822, 2014.

[118] S. K. Hwang and D. H. Liang, "Effects of linewidth enhancement factor on period-one oscillations of optically injected semiconductor lasers," *Appl. Phys. Lett.,* vol. 89, p. 061120, 2006.

[119] T. B. Simpson, F. Doft, E. Strzelecka, J. J. Liu, W. Chang, and G. J. Simonis, "Gain saturation and the linewidth enhancement factor in semiconductor lasers," *IEEE Photon. Technol. lett.,* vol. 13, pp. 776-778, 2001.

[120] C. Henry, "Theory of the Linewidth of Semiconductor Lasers," *IEEE J. Quantum Electron.,* vol. 18, pp. 259-264 1982.

[121] T. Fordell and A. M. Lindberg, "Experiments on the linewidth-enhancement factor of a vertical-cavity surface-emitting laser," *IEEE J. Quantum Electron.,* vol. 43, pp. 6-15, 2007.

[122] G. P. Agrawal, "Effect of gain and index nonlinearities on single-mode dynamics in semiconductor lasers," *IEEE J. Quantum Electron.,* vol. 26, pp. 1901-1909, 1990.

[123] G. P. Agrawal, "Spectral hole-burning and gain saturation in semiconductor lasers: Strong-signal theory," *J. Appl. Phys.*, vol. 63, pp. 1232-1235, 1988.

[124] X. Zhao, D. Parekh, E. K. Lau, H. K. Sung, M. C. Wu, W. Hofmann, M. C. Amann, and C. J. Chang-Hasnain, "Novel cascaded injection-locked 1.55-um VCSELs with 66 GHz modulation bandwidth," *Opt. Express,* vol. 15, pp. 14810-14816, 2007.

[125] H. K. Sung, E. K. Lau, and M. C. Wu, "Optical Single Sideband Modulation Using Strong Optical Injection-Locked Semiconductor Lasers," *IEEE Photon. Technol. lett.,* vol. 19, pp. 1005-1007, 2007.

[126] K. E. Chlouverakis, K. M. Al-Aswad, I. D. Henning, and M. J. Adams, "Determining laser linewidth parameter from Hopf bifurcation minimum in lasers subject to optical injection," *Electron. Lett.*, vol. 39, pp. 1185-1187, 2003.

[127] G. Liu, X. Jin, and S. L. Chuang, "Measurement of linewidth enhancement factor of semiconductor lasers using an injection-locking technique," *IEEE Photon. Technol. lett.,* vol. 13, pp. 430-432, 2001.

[128] C. H. Lin, H. H. Lin, and F. Y. Lin, "Four-wave mixing analysis of quantum dot semiconductor lasers for linewidth enhancement factor extraction," *Opt. Express,* vol. 20, pp. 101-110, 2012.

[129] B. Lingnau, K. Lüdge, W. W. Chow, and E. Schöll, "Failure of the α factor in describing dynamical instabilities and chaos in quantum-dot lasers," *Physical Review E*, vol. 86, p. 065201, 2012.

[130] T. Erneux, V. Kovanis, A. Gavrielides, and P. M. Alsing, "Mechanism for period-doubling bifurcation in a semiconductor laser subject to optical injection," *Phys. Rev. A*, vol. 53, pp. 4372-4380, 1996.